



Deposited via The University of Leeds.

White Rose Research Online URL for this paper:

<https://eprints.whiterose.ac.uk/id/eprint/176383/>

Version: Accepted Version

---

**Article:**

Stubley, SJ, Cayre, OJ, Murray, BS et al. (2021) Enzyme cross-linked Pectin Microgel Particles for Use in Foods. *Food Hydrocolloids*, 121. 107045. ISSN: 0268-005X

<https://doi.org/10.1016/j.foodhyd.2021.107045>

---

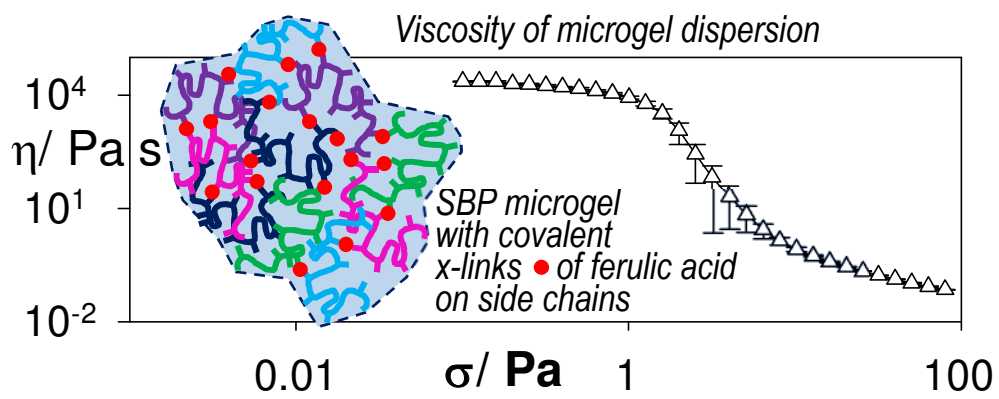
© 2021, Elsevier. This manuscript version is made available under the CC-BY-NC-ND 4.0 license <http://creativecommons.org/licenses/by-nc-nd/4.0/>.

**Reuse**

This article is distributed under the terms of the Creative Commons Attribution-NonCommercial-NoDerivs (CC BY-NC-ND) licence. This licence only allows you to download this work and share it with others as long as you credit the authors, but you can't change the article in any way or use it commercially. More information and the full terms of the licence here: <https://creativecommons.org/licenses/>

**Takedown**

If you consider content in White Rose Research Online to be in breach of UK law, please notify us by emailing [eprints@whiterose.ac.uk](mailto:eprints@whiterose.ac.uk) including the URL of the record and the reason for the withdrawal request.



- Microgels easily prepared via top-down homogenization of pectin gels
- Microgels from  $\text{Ca}^{2+}$ -cross-linked low methoxyl pectin gels unstable (dissolve)
- Microgels from enzymatically cross-linked sugar beet pectin gels highly stable
- Size of sugar beet pectin (*SBP*) microgel particles increases with *SBP* gel strength
- *SBP* microgels show vastly superior thickening cf. *SBP* solutions at same *SBP* conc.<sup>n</sup>

# Enzyme cross-linked Pectin Microgel Particles for Use in Foods

Samuel J. Stubbley<sup>1</sup>, Olivier J. Cayre<sup>2</sup>, Brent S. Murray<sup>1\*</sup>  
Isabel Celigueta Torres<sup>3</sup> & Isabel Fernández Farrés<sup>4</sup>

<sup>1</sup> Food Colloids & Bioprocessing Group, School of Food Science & Nutrition, University of Leeds, UK

<sup>2</sup> Colloid and Polymer Engineering Group, School of Chemical & Process Engineering, University of Leeds, UK

<sup>3</sup> Nestlé Product Technology Centre, York, UK

<sup>4</sup> Nestlé, Nestlé Research Center, Vers-chez-les-Blanc, Switzerland

\* Author for correspondence

**Abstract**

We report on a new enzyme-based method for producing permanently cross-linked pectin microgels. We investigate the shape, size and rheological properties of these microgel particles making comparisons with the more traditional design of calcium cross-linked pectin microgels. Both sets of microgel particles were prepared *via* the 'top-down' mechanical disruption of parent pectin hydrogels. The first hydrogel was prepared from low methoxyl pectin (*LMP*) (2 wt.% pectin) cross-linked using  $\text{Ca}^{2+}$  (8.3 mM  $\text{CaCl}_2$ ). The *LMP* microgels show particle sizes *ca.* 1 to 100  $\mu\text{m}$ , but are stable only in  $[\text{Ca}^{2+}] = 8.3$  mM or above, swelling and/or dissolving rapidly in pure water. The second type of microgel was prepared from sugar beet pectin (*SBP*) hydrogels covalently cross-linked *via* laccase. Gelation kinetics were investigated by small amplitude oscillatory shear rheometry. The *SBP* microgels resisted dissolution in water for several months. Light scattering measurements suggested that the *SBP* microgel particle sizes were related to the mechanical properties of the parent hydrogels. Various imaging techniques all suggested that *SBP* microgels have highly irregular shapes, perhaps due to the top-down technique used for their manufacture and their inherent mechanical properties. Concentrating the *SBP* microgels (to 35 - 50 wt.% microgel, or 0.6 - 0.8 wt.% overall pectin concentration) resulted in suspensions with rheological properties typical of yield stress fluids. When compared at similar overall *SBP* concentrations, the *SBP* microgel suspensions offer distinct advantages as bulk rheology modifiers compared to *SBP* solutions.

**Keywords:** pectin; microgel; laccase; sugar beet; rheology

## 1. Introduction

Hydrogels can be defined as ‘infinitely’ large networks of hydrated polymer molecules which entrap a significant quantity of solvent, either water or electrolyte (Peppas, 1991). In contrast, microgel particles (also referred to as microgels) consist of discrete polymer networks of finite dimensions, swollen by the solvent in which they are dispersed (Pelton & Hoare, 2011). Most (micro)gels with potential applications in foods consist of supramolecular assemblies of biopolymer molecules, more specifically proteins and polysaccharides. Such biopolymers form gels *via* intermolecular association under different conditions with heat set (e.g., globular proteins), cool set (e.g., gelatin and agarose) and ionotropic (e.g., pectins and alginates) gelation mechanisms being most common (Cao & Mezzenga, 2020). This implies that the specific technique employed to synthesize microgels is dependent on the chosen biopolymer characteristics.

Various techniques have been used to manufacture microgels from biopolymers as reviewed elsewhere (Burey, Bhandari, Howes, & Gidley, 2008; Dickinson, 2017; Farjami & Madadlou, 2017; Joye & McClements, 2014; McClements, 2017; Murray, 2019; Shewan & Stokes, 2013). In particular, the mechanical disruption of a bulk hydrogel in the presence of excess solvent holds promise as a scalable technique to prepare microgel particles for industrial food applications and has been widely used for the fabrication of proteinaceous microgels (Guo, et al., 2016; Jiao, Shi, Wang, & Binks, 2018; Matsumiya & Murray, 2016; Sarkar, et al., 2016; Zhang, Holmes, Ettelaie, & Sarkar, 2020). However, this “top-down” approach has been used less frequently for preparing polysaccharide microgels. Ellis and Jacquier (2009) dispersed agarose hydrogels into water by ‘blending’ the mixture with a domestic food processor followed by rotor-stator mixing at various operating speeds and durations to obtain agarose microgel suspensions (Ellis & Jacquier, 2009). Saavedra Isusi *et al.* (2019) fabricated pectin microgel particles based on low-methoxyl pectin (*LMP*), amidated *LMP* and polygalacturonic (pectinic) acid. The pectin hydrogels were fragmented in excess water *via* sequential rotor stator mixing and wet milling to yield microgel particles (Saavedra Isusi, Karbstein, & van der Schaaf, 2019). Note that the mechanism of particle generation *via* the methods used here are different to the production of shear (fluid) gels. In fluid gel formation, biopolymer solutions are *simultaneously* sheared and gelled, so that the final gel particle size is a result of the competition between network formation (i.e., particle growth) and network break-up due to the imposed flow field (Fernández Farrés & Norton, 2014).

Pectins, in particular, have a long history of being used as a gelling agent in foods. They are generally extracted from agro-industrial waste streams (e.g., apple pomace and citrus pulp) and are therefore widely available at a reasonable cost (May, 1990). Thus, they are an ideal polysaccharide to develop food-grade microgel preparations. Applications could include: texture modification for desirable rheological and/or sensory responses (Shewan, Stokes, & Smyth, 2020; Stokes, 2011), stabilization of Pickering emulsions and foams (Dickinson, 2017; Murray, 2019) and the encapsulation of water-soluble pigments, bioactive or flavour molecules (McClements, 2017).

Pectin molecules have chemical structures analogous to block copolymers, with three distinct types of region: homogalacturonan (*HG*), rhamnogalacturonan I (*RGI*) and rhamnogalacturonan II (*RGII*). The *HG* domain consists of 1,4-linked  $\alpha$ -D-galacturonic acid (*GalA*) residues in which some of the carboxyl groups may be esterified at C6 by methyl groups. Degrees of methyl esterification above and below 50% correspond to high-methoxyl (*HMP*) or low-methoxyl (*LMP*) pectins, respectively. The rhamnogalacturonan domains (*RGI* and *RGII*) are more structurally complex and are colloquially referred to as the “hairy regions” due to the presence of pendant sugar side chains (May, 1990). The *RGII* domain contains heteroglycan side chains covalently bound directly to a *HG* backbone (Ishii & Matsunaga, 1996). In contrast, the *RGI* backbone consists of alternating *GalA* and  $\alpha$ -L-rhamnopyranose units as a repeating disaccharide. The rhamnose residues in this region bear neutral sugar side chains mainly composed of arabinose and galactose (Renard, Crépeau, & Thibault, 1995).

The mechanism of gelation in pectins is related to their fine structure and the solvent composition. For example, gelation of *LMP* (at  $\text{pH} > \text{pK}_a$ ) is usually achieved by the addition of divalent cations, principally  $\text{Ca}^{2+}$ , and cross-linking occurs in the *HG* region. It is estimated that 6 to 13 consecutive non-esterified galacturonic acid residues are required for the formation of a stable junction zone (Luzio & Cameron, 2008). If this condition is satisfied, polyanionic pectin chains can be bridged by divalent cations according to the (shifted) egg-box model (Braccini & Pérez, 2001) originally developed to explain the ionotropic gelation of alginates (Grant, Morris, Rees, Smith, & Thom, 1973).

The fine structure of pectins further depends on the botanical source and conditions of extraction. For example, sugar beet pectins (*SBP*) are generally extracted as *HMP* and contain acetyl groups esterified to the secondary alcohols of *GalA*, primarily in the *HG* region (Ralet, et al., 2005). The high degree of substitution renders *SBP* incompatible with the conventional gelation mechanisms described above without chemical modification to remove some methyl and/or acetyl groups

(Matthew, Howson, Keenan, & Belton, 1990; Oosterveld, Beldman, Searle-van Leeuwen, & Voragen, 2000; Phippen, McCready, & Owens, 1950; Williamson, et al., 1990). *SBP* is also known to contain ferulic acid (*FA*) residues esterified to the neutral sugar side chains of *RGI*. This is important because the *FA* moieties can covalently cross-link discrete pectin molecules *via* oxidative coupling reactions. Under conditions favorable for network development, *chemical* hydrogels can be generated in this way without the need for removal of methyl or acetyl esters. Such reactions require the generation of free radicals and the use of an effective oxidizing system such as (ammonium) persulfate (Guillon & Thibault, 1987, 1990; Oosterveld, Beldman, & Voragen, 2000; Thibault, Garreau, & Durand, 1987; Thibault & Rombouts, 1986), peroxidase enzymes in combination with hydrogen peroxide (Norsker, Jensen, & Adler-Nissen, 2000; Oosterveld, Beldman, & Voragen, 2000; Zaidel, Chronakis, & Meyer, 2012) or laccases (Kuuva, Lantto, Reinikainen, Buchert, & Autio, 2003; Micard & Thibault, 1999; Norsker, et al., 2000; Zaidel, et al., 2012). In all cases, the oxidation of polymer bound *FA* and subsequent coupling of phenoxyl radicals results in cross-linking of pectin chains *via* *FA* dimers and/or higher ferulate oligomers (Bunzel, 2010).

A critical number of cross-links is required for the sol-gel (liquid-solid) transition and the efficient formation of a hydrogel. The tendency for network development in *SBP* solutions will therefore depend on the number of *FA* residues and their ability to participate in oxidative coupling reactions. However, not all *FA* residues are necessarily able to participate in cross-linking due to their location within the neutral sugar side chains of *RGI*. The galactan side chains of *SBP* mostly consist of linear  $\beta$ -1,4 linked galactopyranose residues esterified by *FA* at O-6 (Colquhoun, Ralet, Thibault, Faulds, & Williamson, 1994). In contrast, arabinan side chains are highly branched consisting of a main core of  $\alpha$ -1,5 linked arabinofuranose (*Araf*) residues, randomly substituted by individual or short chains of  $\alpha$ -1,3 linked *Araf* (Guillon, Thibault, Rombouts, Voragen, & Pilnik, 1989). Within arabinan side chains, *FA* is primarily found to be ester linked to *Araf* residues in the main core at O-2 (Colquhoun, et al., 1994). Hence, the presence of neutral sugar branches might sterically hinder the coupling of phenoxyl radicals. For example, it has been shown that gelation of *SBP* can be promoted following treatment with arabinase enzymes to remove some peripheral *Araf* residues (Guillon, et al., 1987; Micard, et al., 1999).

To be successfully incorporated into commercial formulations, microgel particles must retain their structural integrity throughout any subsequent manufacturing steps, storage and consumer handling. Thus, chemically acceptable cross-linking might be preferable to physical cross-linking in

terms of providing a more stable internal structure and more robust particles. Indeed, the mechanical properties of physically cross-linked gels vary with environmental conditions such as ionic strength, pH and temperature (Djabourov, Nishinari, & Ross-Murphy, 2013). In the current study we report on the fabrication of *SBP* microgels (*SBPM*) using a top-down technique involving the mechanical disruption of a chemically cross-linked *SBP* hydrogel. To our knowledge, this is the first example of a covalently cross-linked polysaccharide microgel prepared in this way. For comparison, we also present data for calcium cross-linked *LMP* microgels prepared in a similar fashion and provide insight into how their (long-term) stability can be improved.

## 2. Materials and Methods

### 2.1. Materials

Sugar beet pectin (GENU® Beta Pectin) and amidated low methoxyl citrus pectin (GENU® Pectin LM-104 AS), hereafter referred to as *SBP* and *LMP*, respectively, were a generous gift from CP Kelco (Lille Skensved, Denmark). Laccase Y120 (EC 1.10.3.2) was obtained from Amano Enzyme (Nagoya, Japan). Fluorescein isothiocyanate-dextran (average molecular weight  $2 \times 10^6$  Da), sodium azide and 2,2'-azino-di-(3-ethylbenzthiazoline sulfonic acid) (*ABTS*) were obtained from Sigma Aldrich (Dorset, UK). Crystal violet was obtained from Fluorochem Ltd (Hadfield, UK). Citric acid, trisodium citrate dihydrate, monosodium phosphate monohydrate and calcium chloride dihydrate were of analytical grade from Sigma Aldrich. Silicone oil with viscosity of 350 centistokes (cSt) and 20 cSt were obtained from VWR International (Paris, France) and BDH Silicone Products (Poole, UK) respectively. Type I (Milli-Q) water (Millipore, Bedford, UK) with a minimum resistivity of 18.2 M $\Omega$ .cm was used throughout.

### 2.2. Methods

#### 2.2.1 Fabrication of *LMP* hydrogels and microgel suspensions

*LMP* powder was used as supplied and dissolved in 10 mM trisodium citrate solution at a concentration of 2.4 wt.% *via* magnetic stirring for a minimum of 12 h at room temperature. *LMP* and 50 mM CaCl<sub>2</sub> solutions were separately decanted into sealed glass containers, transferred to a shaking water bath (OLS Aqua Pro, Grant Instruments, Cambridge, UK) set to 85 °C at 20 rpm and pre-heated for 30 min.

Gelation of 25 ml of *LMP* solution was initiated *via* the ‘one-shot’ addition of 5 ml of  $\text{CaCl}_2$  stock solution with gentle shaking to prevent the formation of air bubbles. Containers were sealed and the gelling mixture was allowed to cool to ambient temperature and subsequently refrigerated for a minimum of 12 h. *LMP* hydrogels containing 2 wt.% *LMP*, 8.34 mM  $\text{CaCl}_2$  and 8.33 mM sodium citrate were subsequently used for the fabrication of *LMP* microgels. These conditions were reached by trial and error until reproducible, clear, homogeneous gels were obtained without any noticeable syneresis. Higher concentrations of  $\text{CaCl}_2$  led to visible gel inhomogeneity. The influence of calcium concentration on the physiochemical properties of *LMP* hydrogels is often evaluated based on the stoichiometric ratio ( $R$ ) of calcium ions to non-methoxylated *GalA* residues through  $R = 2[\text{Ca}^{2+}]/[\text{COO}^-]$ . The typical degree of methoxylation ( $DM$ ) and degree of amidation ( $D_{AM}$ ) are given in Table 1, as specified by the manufacturer and these values were also used to guide the choice of gelation conditions.

*LMP* microgel suspensions were prepared via mechanical disruption of 20% volume fraction ( $\phi_{\text{gel}}$ ) of coarse *LMP* hydrogel pieces in the presence of excess solvent, hereafter referred to as the dispersion medium. Two different dispersion media were tested: Milli-Q water and 8.34 mM  $\text{CaCl}_2$  aqueous solution. Two types of disruption were tested. The first was using a T25 ULTRA-TURRAX (IKA, Oxford, UK) rotor-stator device, equipped with a (S25N - 18G dispersing tool (gap between rotor and stator = 0.3 mm) operating at a speed of 10,000 rpm for 10 min. The second disruption method utilized firstly a Silverson blender (Model L5MA, Silverson Machines, Buckinghamshire, UK) equipped with a general purpose disintegrating head, operated at 2000 rpm for 60 s, followed by further disruption by passing the dispersion through a high-pressure valve homogenizer (Panda Plus 2000, GEA Niro Soavi Homogeneizador, Parma, Italy), pre-set with water to operate at 350 bar. The pressure was found to fluctuate slightly with the dispersions but did not exceed 500 bar. Samples were passed through this homogenizer a total of 3 times. This second method was an attempt to create smaller *LMP* microgel particles – see Results below. Where microgel suspensions were stored for prolonged periods of time, sodium azide was added at a concentration of 0.005 wt.% to suppress microbial growth.

### 2.2.2 Fabrication of *SBP* hydrogels and microgel suspensions

The concentrations of *SBP* and laccase used were initially optimised for the generation of homogeneous hydrogels displaying no noticeable syneresis on storage for several days. *SBP* powder

was dispersed into water using the T25 ULTRA-TURRAX operating at a maximum speed of 15000 rpm, adding the powder gradually to prevent clumping. *SBP* was left to solubilize for a minimum of 12 h with magnetic stirring in sealed glass jars. The *SBP* solutions were then centrifuged (Eppendorf 5810 R, Stevenage, UK) at 4000 rpm for 60 min in approximately 30 ml aliquots to remove any remaining insoluble material. Laccase stock solutions were freshly prepared by solubilizing the enzyme powder in water for a minimum of 20 min. 25 ml of *SBP* solution and 5 ml of laccase stock solution were rapidly combined at ambient temperature by vortex mixing. When the two solutions were visibly well mixed, hydrogels were allowed to develop quiescently in sealed containers for a minimum of 12 h at 25 °C.

The influence of *SBP* and enzyme concentrations, hereafter referred to as  $C_{GEL}$  and  $C_E$  respectively, on the mechanical properties of the resulting hydrogels was investigated. In order to determine the actual values of  $C_{GEL}$ , the gelation procedure outlined above was simulated by replacing enzyme solutions with water and drying the diluted *SBP* solutions in a vacuum oven (Townson and Mercer Limited, Croydon, England) at 75 °C and a pressure of 600 mm Hg until no change in mass was observed. This technique was preferred over drying the hydrogels and allowed us to account for losses due to: potential incomplete solubilization of *SBP* powder, any insoluble material removed by centrifugation and any water associated with the powder before preparing the solutions. The same drying procedure was also used to determine the overall pectin concentration,  $C_{PTOTAL}$ , in any microgel suspensions or *SBP* solutions investigated.

*SBP* microgels (*SBPM*) were obtained from parent hydrogels prepared by the addition of laccase at a nominal  $C_E$  of 0.1 mg ml<sup>-1</sup> followed by a 12 h storage period. Unless otherwise stated, *SBPM* suspensions were fabricated by blending a 20% volume fraction ( $\phi_{gel}$ ) of the hydrogel with deionized water in the ULTRA-TURRAX rotor-stator, i.e., as for the *LMP* microgels described above. Just one set of *SBPM* suspensions was created slightly differently, using the Silverson blender method as used for the *LMP* microgels described above (but without the second stage valve homogenization), for comparison with the results of the ULTRA-TURRAX method and also the *LMP* microgels. Sodium azide (0.005 wt.%) was added as a preservative after the fabrication of the microgel suspensions and to inhibit any further enzyme activity. Centrifugation was used to concentrate the *SBPM* suspensions for rheological characterization and investigations via microscopy. Suspensions were centrifuged at 4,000 rpm for 60 min to obtain a pellet of microgel particles and the supernatant was subsequently discarded.  $C_{PTOTAL}$  was determined from a diluted sample of the pellet as described for in section 2.2.2.

### 2.2.3 Equilibrium swelling of SBP hydrogels

Approximately 2 ml of a gelling pectin solution, mixed with enzyme to give  $C_E = 0.1 \text{ mg ml}^{-1}$ , was transferred to 5 ml disposable syringes with the tips cut off to act as a cylindrical mould. Syringes were covered with Parafilm® and incubated in an upright position at 25 °C for at least 12 hours. The initial mass  $M_0$  of the hydrogel was determined to two decimal places by transfer to 50 ml centrifuge tubes containing 15 ml of deionized water at pH 6. The mass  $M$  of hydrogels after a specified time in contact with the swelling medium was determined after draining excess water from the surface of hydrogel cylinders with filter paper and re-weighing. The 'final' ratio of  $M/M_0$  was defined as the swelling ratio,  $S$ . Reported values of  $S$  are based on at least two measurements. Due to the delicate nature of these hydrogels, particularly when swollen, it was not possible to track the increase in mass over time on the same hydrogel. Rather, hydrogels were swollen in "pairs", each pair being discarded after measuring  $M$ .

### 2.2.4 Enzyme (laccase) activity assay via UV/VIS spectrophotometry

A Specord® 210 PLUS UV/VIS spectrophotometer (Analytik Jena, Jena, Germany) was used to perform enzyme assays. The relative enzyme activity was measured by monitoring the oxidation of ABTS substrate *via* absorbance measurements at  $\lambda = 420 \text{ nm}$  for 10 min at 25 °C. Disposable cuvettes with a path length of 1 cm were used. The final reaction volume (3 mL) contained 2 mM ABTS and (10  $\mu\text{L}$ ) of enzyme stock solutions, both of which were prepared in McIlvaine buffer (pH 3).

### 2.2.5 Particle size analysis by laser diffraction

A Mastersizer 3000 equipped with the Hydro EV wet sample dispersion unit (Malvern Instruments, Worcestershire, UK) was used to perform laser diffraction measurements on all pectin microgel samples at ambient temperature (20 °C). After optical alignment and measurement of background scattering, microgel samples were added to the dispersion unit until the laser obscuration reached > 1%. Particle size distributions (*PSD*) are inferred in the Mastersizer software from the angular dependence of scattered light intensity via the Mie theory for spherical particles. As such, knowledge of the optical properties of the dispersant and dispersion medium is required. The Mastersizer dispersion medium was water (refractive index = 1.33). For both *LMP* and *SBP* microgels,

a refractive index of 1.35 (Nikolova, Panchev, & Sainov, 2007) and an absorption index of 0.01 was used. Representative *PSDs* are reported alongside mean values of particle diameter, namely the Sauter (surface weighted) mean diameter  $D_{3,2}$  and the volume weighted mean diameter  $D_{4,3}$ , calculated according to;

$$D_{a,b} = \frac{\sum n_i D_i^a}{\sum n_i D_i^b} \quad (1)$$

Where  $n_i$  is the number of particles of diameter  $D_i$ . The width of the *PSD* is reported in terms of the *Span*;

$$Span = \frac{Dv_{90} - Dv_{10}}{Dv_{50}} \quad (2)$$

Where  $Dv_x$  is the diameter of which x percentage of particles are smaller. All values reported are based on the average of 5 measurements on each individual sample.

#### 2.2.6 Microscopy of SBPM suspensions

A Zeiss confocal laser scanning microscope (*CLSM*) (Model LSM 700, Carl Zeiss Microscopy GmbH, Jena, Germany) with a 40x/NA1.4 oil immersion lens was used to image *SBPM* particles. A reverse contrast method was employed whereby FITC-dextran (0.1 wt. %), used to stain the continuous phase, was dissolved directly into the microgel suspensions before transfer to microscope well slides for imaging. The wavelengths of excitation and emission used were 488 and 528 nm, respectively. Standard transmission optical microscopy was performed using a Nikon SMZ-2T light microscope (Nikon, Japan) equipped with a 10x objective lens. To improve contrast between the continuous phase and solvent swollen microgel particles, crystal violet was used to stain suspensions by adding a few drops of an 0.5 wt.% crystal violet stock solution to 30 ml of suspension. Stained suspensions were gently stirred for one hour, concentrated by centrifugation and placed in well slides. Images were captured with a digital camera (Leica MC120 HD) and scale bars were added in ImageJ.

For scanning electron microscopy (*SEM*), samples were encapsulated in a 3 wt% agar gel in a plastic tube. The tube contents were fixed by curing for over 8 h in 3.7 wt% formaldehyde solution. The aqueous phase was then replaced by ethanol *via* successive immersion in baths with increasing ethanol concentration (10 %, 30 %, 50 %, 70 %, 90 % and 100 %). The sample was then dried by immersion in supercritical CO<sub>2</sub>, followed by release to atmospheric pressure. The sample tubes were cut transversely, and the thin sections glued onto an *SEM* stub and coated with a 10 nm gold layer,

then imaged in low vacuum mode *via* a Quanta F200 Scanning Electron Microscope. This SEM sample preparation has been validated elsewhere (Allan-Wojtas & Kalab, 1984; Kalab, 1988).

### 2.2.9 Rheology of SBP solutions, hydrogels and microgel suspensions

An Anton Paar MCR 302 (Anton Paar GmbH, Graz, Austria) rheometer was used for all shear rheology experiments and all raw data were analyzed in the RheoCompass software. For gelation kinetics, a small volume of the SBP + laccase solution was immediately transferred to the gap between a 50 mm parallel plate measuring set (PP50), with the gap set to 1 mm. The measurement geometry was covered by a custom-made circular plastic hood with dampened kitchen roll fixed to its inner circumference to prevent solvent evaporation. For experiments > 80 min long, 350 cSt silicone oil was used as a solvent trap in addition to the hood. Dynamic viscoelasticity was monitored with time  $t$  at 25 °C at a frequency of 1 Hz and a strain amplitude of 0.1 % (well within the linear viscoelastic region (LVER) of the final hydrogels - data not shown). Data were recorded every 30 s for 60 to 240 min. Amplitude sweeps (at 1 Hz) were also performed on some hydrogels as they formed *in situ*.

Flow curves for SBP solutions were measured at 20 °C using a cone-plate measuring set (CP75): 75 mm diameter cone, 1° cone angle and 151  $\mu\text{m}$  gap. A 20 cSt silicone oil solvent trap was used to prevent solvent evaporation. Samples were pre-sheared at a shear rate of 50  $\text{s}^{-1}$  for 30 s, left at rest for 5 min, then a logarithmic shear stress ramp applied with 10 data points recorded per decade on reaching steady state reached or after a maximum duration of 5 min at each applied stress.

The PSD of the SBPM precluded the use of the same cone-plate measuring set to measure the rheology of these dispersions. Roughened parallel plates (50 mm diameter) were used, since wall-slip appeared to be an issue in preliminary measurements around the apparent yield stress of some dispersions when using smooth plates (data not shown). The plates were roughened by gluing water-resistant silicon carbide sandpaper (600 grit, from 3M) to both the upper and lower plates *via* a multi-purpose silicone rubber sealant (Dow Corning 732), followed by curing for a minimum of 12 h. The sample was loaded and the gap set to 1 mm. Samples were then pre-sheared at a shear rate of 50  $\text{s}^{-1}$  for 30 s, left at rest for 15 min, then a logarithmic shear stress ramp applied as above for the SBP solutions.

## 3. Results and Discussion

### 3.1 Amidated low methoxyl pectin (LMP) microgels

Calcium cross-linked *LMP* microgels were prepared as described in section 2.2.1, using two different dispersion media: pure water and 8.34 mM  $\text{CaCl}_2$  aqueous solution. Note that the  $[\text{Ca}^{2+}]$  in the latter matches that used to form the hydrogels in the first place. It was expected that the different media would induce different degrees of microgel swelling, by analogy with bulk gels (Djabourov, et al., 2013). In particular, *LMP* hydrogels physically cross-linked *via*  $\text{Ca}^{2+}$ , when placed in pure water or NaCl solutions, can undergo pronounced swelling that progressively leads to complete gel dissolution as the cross-linking multivalent cations are replaced with monovalent cations from the bulk (Sriamornsak & Kennedy, 2008).

Fig. 1 shows the *PSD* of the *LMP* microgels and Table 2 gives the corresponding characteristics of these *PSDs*. Fig. 1A shows the *PSD* of the *LMP* microgels created via the ULTRA-TURRAX in 8.34 mM  $\text{CaCl}_2$ , dispersed in Mastersizer tank (in water) and measured after 1 and 60 min. During this time there was a distinct shift in the *PSD* to lower sizes, as reflected in the mean particle sizes in Table 2. Further analysis of the changes in a diluted dispersion of these particles was carried out during the laser diffraction measurement of their size distribution (Fig. S1). The evolution of the size distribution and the laser obscuration of the sample over 60 min shows an apparent increase followed by a decrease in particle size. These changes were attributed to initial swelling of the *LMP* microgels in water, followed by their dissolution. The bulk *LMP* hydrogels were observed to swell significantly over 24 h when incubated in excess water at room temperature (data not shown). It is likely that the sodium citrate, included as a  $\text{Ca}^{2+}$  chelating agent to slow down and assist in the production of homogeneous *LMP* hydrogels, increased this swelling, as previously observed by others (Gombotz & Wee, 1998).

Fig. 1B shows the *PSD* of the *LMP* microgels created via the two step Silverson blender + valve homogenizer method, with Milli-Q water or 8.34 mM  $\text{CaCl}_2$  as the dispersion medium during fabrication of the microgels from the hydrogels. Much smaller particle sizes were obtained ( $D_{90} = 1.17 \mu\text{m}$ ) when the microgels were fabricated in water with a reasonably narrow, monomodal *PSD* (*Span* = 0.963). However, because of the previous results in Fig. 1A described above, it is not clear if this *PSD* represents microgels that were created in this size range in the homogenizer, or microgels that have rapidly undergone significant dissolution in water, due to a smaller initial size and therefore much higher surface area to volume ratio (McClements, 2017).

On the other hand, Figure 1B also shows that, when the same two step Silverson blender + valve homogenizer method is used but the hydrogel is broken down to microgels in 8.34 mM  $\text{CaCl}_2$ , i.e., the same  $[\text{Ca}^{2+}]$  used to cross-link the parent hydrogel, a *PSD* at much larger particles sizes is observed in comparison to when the microgels are created in water only. In fact this *PSD* is similar to that obtained with the ULTRA-TURRAX and  $D_{32}$ ,  $D_{43}$  AND  $D_{90}$  are only slightly smaller as a result of the two step method (see Table 2), despite the latter method being expected to exert higher mechanical stresses. More importantly, this *PSD* did not change over time. The data in Table 2 corroborates that the mean particle size and Span are much larger than for the *LMP* microgels dispersed in water - some particles were even visible to the naked eye, but these persisted for at least 7 days – whilst the residuals value was much smaller, suggesting a better measurement quality. These measurements likely represent the *PSD* of the microgels in their most swollen state, assuming no dissolution has already taken place. The apparent *PSDs* could also be influenced by the presence of naturally occurring molecular aggregates often found in these systems (Berth, Dautzenberg, & Hartmann, 1994; Smith & Stainsby, 1977; Sorochan, Dzizenko, Bodin, & Ovodov, 1971). For the calcium cross-linked pectin microgel particles fabricated by Saavedra Isusi et al. (2019), a wet milling procedure resulted in a larger particle size (and therefore lower surface area to volume ratio) when compared to the microgels prepared *via* the valve homogenization in our study. The authors stated that their microgel particles resisted swelling over a period of 24 h, although no data was provided (Saavedra Isusi, et al., 2019).

All in all, the data suggested that it was difficult to conclude whether the *PSDs* in water represented swollen but highly dissolved *LMP* microgels or *LMP* molecular aggregates. On the other hand, the *PSDs* in the more  $\text{Ca}^{2+}$ -rich dispersion medium seemed more likely to represent 'true' microgel particles, since this dispersion medium apparently prevented the *LMP* microgel particle dissolution. It should also be noted that, bulk *LMP* hydrogels immersed in 8.34 mM  $\text{CaCl}_2$  for 24 h at room temperature did not visibly swell (data not shown). Clearly, the high pressure homogenization must break some junction zones in converting the macro-sized gel pieces to microgels, but it is also possible in the high shear conditions that junction zones within the nascent microgels particles are momentarily disrupted but rapidly reform (in the same or different location), since the released  $\text{Ca}^{2+}$  ions will still be in the vicinity. This will affect the final form and mechanical properties of the microgel particles, so that the latter might be significantly different from the original bulk gel.

However, this will be difficult to prove unless micromechanical measurements on individual microgel particles were made, which is beyond the scope of this study.

In addition, the exact osmotic pressure difference between the inside and outside of the microgels will influence their degree of swelling and how much this disrupts the junction zones. Placing the microgels in more 'salty' solutions could lead to their shrinkage but also to ion exchange and further microgel disruption. Being restricted to tight control of the microgel environment to ensure stability would be a significant challenge for practical applications, which would therefore limit their usefulness. On the other hand, the apparently stable calcium cross-linked *LMP* microgels dispersed in 8.34 mM  $\text{Ca}^{2+}$  may have some useful applications. For example, transfer to physiological fluids could result in changes in particle swelling making the system a possible candidate for drug delivery (Peppas, 1991). The dissolution of such microgels is likely to accelerate on heating, since this is what occurs in the case of bulk  $\text{Ca}^{2+}$  cross-linked hydrogels. This would be a disadvantage if the particles are required to survive pasteurization, but an advantage if simple heating can be used to release materials that they encapsulate. Immersion in higher  $[\text{Ca}^{2+}]$  might allow further strengthening of the microgel particle surface if the pectin carboxylate groups are not fully saturated with  $\text{Ca}^{2+}$  ions. However, this is outside the scope of this article, which aims to use these physically cross-linked microgels as a comparison for chemically cross-linked microgel particles that are predicted to be more robust.

### 3.2 Sugar beet pectin hydrogels

#### 3.2.1 Assay of laccase enzyme activity

Fig. S2 shows the relative activity of the laccase enzyme preparation used to catalyse the oxidative cross-linking of *SBP* as measured *via* the *ABTS* assay at different nominal enzyme concentrations ( $C_E$ ). The absorbance ( $A$ ) over time was linear for all  $C_E$  ( $R > 0.996$  in all cases). Using the data between 0 and 300 s to calculate reaction rates ( $dA/dt$ ) gave  $1.89$ ,  $3.51$  and  $6.07 \times 10^{-3} \text{ s}^{-1}$  for  $C_E = 0.15$ ,  $0.30$  and  $0.50 \text{ mg ml}^{-1}$  laccase, respectively, as shown in the inset to Fig. S2. It was not considered relevant to examine the enzyme kinetics in any more detail, since all that we wished to establish was the approximate relative activity of the enzyme with respect to  $C_E$ . The more important data were how different enzyme activities affected the kinetics of *SBP* gelation, as discussed below.

#### 3.2.2 Gelation kinetics of *SBP* hydrogels

In early studies on *SBP* gelation, the gel state was often evaluated based on simple qualitative tube inversion test and visual inspection (Guillon, et al., 1990; Micard, et al., 1999). More recently, rheological techniques have been used to characterize *SBP* hydrogels (Kuuva, et al., 2003; Norsker, et al., 2000; Oosterveld, Beldman, & Voragen, 2000; Zaidel, et al., 2012) prepared under different conditions. The rate of gelation as well as the final, equilibrium mechanical properties of the *SBP* hydrogels are expected to influence the properties of the corresponding microgels, for example their average particle size and particle elasticity. In small amplitude oscillatory shear experiments, the plateau value of the elastic shear modulus ( $G'$ ) is proportional to the number of intermolecular cross-links (Ross-Murphy, 1995). Thus, studying the evolution of  $G'$  over time at a constant frequency (1 Hz) and strain amplitude within the LVER for the final hydrogels potentially allows one to monitor the rate and extent of cross-linking, which may be affected by both  $C_{PTOTAL}$  and  $C_E$ . Such experiments also enabled the development of robust protocols to obtain hydrogels compatible with the top-down technique for microgel formation.

Fig. 2A shows the evolution of  $G'$  over time for 2.4 wt.% *SBP* hydrogels prepared at different  $C_E$ ; 0.1, 0.2 and 0.4 mg ml<sup>-1</sup>, respectively. This figure suggests that the kinetics of network development are dose-dependent with respect to  $C_E$ . The 'final' values of  $G'$  tended towards a common value of around 200 Pa at the end of the experimental time frame, which suggests that most available ferulic acid residues have been consumed, i.e., the system was approaching the maximum possible cross-linking. Rheological measurements at longer times were difficult due to samples drying out, despite the use of a cover or solvent trap. We therefore attempted to fit the data to a kinetic model that allows 'extrapolation' to a final equilibrium value of  $G'$  ( $G'_{inf}$ ). This kinetic model has been successfully applied previously to heat-denatured protein gels setting at constant temperature (Gosal, Clark, & Ross-Murphy, 2004; Loveday, Su, Rao, Anema, & Singh, 2011):

$$G' = G'_{inf} \exp(-B/t) \quad (3)$$

where  $t$  is time and  $B$  is the kinetic constant, which is lower for faster increase in  $G'$ .  $G'_{inf}$  is a constant that reflects  $G'$  when  $t \rightarrow \infty$  and therefore the exponential terms tends to zero.  $G'_{inf}$  and  $B$  were determined by non-linear regression fits of equation 3 to the data, shown in Fig. S3.

Table 3 shows the fitted  $G'_{inf}$  and  $B$  - the residuals were small in all cases (see Fig. S3). For the same  $C_{GEL} = 2.4$  wt.% but 3 different  $C_E$  (0.1, 0.2. and 0.4 mg ml<sup>-1</sup>)  $G'_{inf}$  were similar but decreased slightly with increasing  $C_E$ . It has been suggested that, when cross-linking is too rapid, the final cross-link

density (and thus the gel strength and  $G'$ ) can be reduced (Kuuva, et al., 2003; Zaidel, et al., 2012). Indeed, rapid cross-linking can restrict the motion and flexibility of the cross-linked pectin molecules and their neighbours, such that further cross-linking is frustrated. In agreement with this, it was also observed that with  $C_{GEL} = 2.4$  wt.% *SBP* and  $C_E > 0.4$  mg/ml, gelation was even more rapid but lower long-time values were obtained (data not shown). Furthermore, such hydrogels exhibited significant syneresis on storage, which is also indicative of a coarser gel network, but also suggested that they were not suitable for producing microgel particles with uniform  $G'$ . For this reason, in order to create uniform hydrogels and microgels with a range of different mechanical properties, it is probably best to vary  $C_{GEL}$  once an optimum of  $C_E$  has been established.

Using both the laccase/ $O_2$  and peroxidase/ $H_2O_2$  oxidizing systems, Zaidel et al. (2012) showed that above a certain enzyme activity  $G'$  tended towards a common value after 20 min, similar to the experimental values in Fig. 2A. For example, 2.5 wt.% *SBP* + 2 U ml<sup>-1</sup> laccase resulted in a value of  $G' \approx 300$  Pa at  $t \approx 20$  min. However, the data from Zaidel et al. (2012) showed that  $G'$  was still increasing slightly after this time, as observed in our results. Using laccases from *Trametes hirsute* and an *SBP* concentration of 1.5 wt.%, Kuuva et al. (2003) reported similar findings and no plateau in  $G'$  was reached after 5.5 h. Interestingly, Kuuva et al. (2003) found that at high  $C_E$  the addition of  $CaCl_2$  slowed down the rate of increase in  $G'$  but a higher final value of  $G'$  was reached. It is unclear whether this was due to ionic cross-linking between  $Ca^{2+}$  and *HG* regions of *SBP* or an effect of  $Ca^{2+}$  on the enzyme activity, although there was no gelation in the absence of enzyme (Kuuva, et al., 2003).

It is seen that  $C_E$  mainly affects the gelation kinetics: as  $C_E$  increases this leads to a more rapid increase in  $G'$ , reflected in a clear trend in the kinetic constant  $B$ , that is lowest for faster kinetics - see Table 3. For example,  $B = 677, 1226$  and  $2515$  s for  $C_E = 0.4, 0.2$  and  $0.1$  mg ml<sup>-1</sup>, respectively. Zaidel et al. (2012) also showed that the rate of *SBP* gelation was dose-dependent with the rate of cross-linking increasing with  $C_E$ . Table 2 shows that the final gel strength is determined largely by  $C_{GEL}$  and not  $C_E$  at least in this range of concentrations. Indeed, there is a clear and sharp increase in  $G'_{inf}$  with increasing  $C_{GEL}$  at fixed  $C_E$  (0.1 mg ml<sup>-1</sup>) rising from 293 to 1286 Pa between  $C_{GEL} = 2.4$  and 4.0 wt.%, which has been shown previously (Oosterveld, Beldman, & Voragen, 2000). The trend with  $C_{GEL}$  is similar to heat-set gels (Ross-Murphy, 1995) but, due to the absence of data points at a wider range of  $C_{GEL}$ , we have not attempted to extract a critical gelation concentration (i.e., the minimum pectin concentration for gelation to take place) from these data,. Nevertheless, the universality of the gelation mechanism can be illustrated by scaling each  $G'$  vs  $t$  curve with the appropriate kinetic

constants  $G'_{inf}$  and  $B$ , respectively, as shown in Fig. 3. Either at fixed  $C_{GEL}$  and varying  $C_E$  (Fig. 3A) or fixed  $C_E$  and varying  $C_{GEL}$  (Fig. 3B) all the data superimpose very well onto a master curve. This gives added credence to the appropriateness of the model. Gosal et al. (2004) and Loveday et al. (2011) observed the same type of scaling for their data on heat-set protein gels, suggesting that the time-dependent formation of enzyme-driven covalent cross-links proceeds in a similar fashion to the formation of strong bonds between elements of unfolded proteins when forming a network.

### 3.2.3 Equilibrium swelling of sugar beet pectin (SBP) hydrogels

Fig. 4 shows that the laccase-cross-linked *SBP* hydrogels swelled in water to different extents, depending on  $C_{GEL}$ . In contrast to the  $Ca^{2+}$  cross-linked *LMP* hydrogels, none of the *SBP* hydrogels dissolved, likely as a result of the the permanence of covalent cross-links. Indeed, hydrogel cylinders incubated in 0.005 wt.% sodium azide solution for > 1 month resisted any dissolution and retained their cylindrical shape. The rate and extent of swelling depends on factors such as intermolecular cross-link density, temperature, solvent quality and dilution factor (McClements, 2017). Within experimental error the swelling ratio  $S$ , indicated by the dashed horizontal lines in Fig. 4, was constant after 18 to 24 h and decreased in the order  $1.42 < 1.45 < 1.50$  for  $C_{GEL} = 4.0 < 3.4 < 2.4$  wt.%, respectively. This observed decrease, in order of increasing  $G'_{inf}$ , is expected if the cross-link density increases with  $C_{GEL}$ . The values of  $S$  were used to calculate the final wt.% concentration of microgel particles,  $C_{MG}$ , in any subsequent dispersion from:

$$C_{MG} \text{ (wt.\%)} = 100 \times S \times C_{PTOTAL} / C_{GEL} \quad (4)$$

where  $C_{PTOTAL}$ , the total pectin concentration in a given sample of microgel suspension, was determined by vacuum drying as described for  $C_{GEL}$  in section 2.2.2. Note this calculation assumes that no pectin is lost from the bulk hydrogel in its conversion to microgel particles. Like the *LMP* microgels, equilibrium swelling of the *SBPM* was assumed to be reached much more rapidly than the hydrogels, due to their much higher surface area to volume ratio. Certainly, equilibrium swelling was expected to be achieved within the time before which the microgels were analyzed for their particle size and rheological properties (see below) and no significant changes in microgel particle size with time were observed in either the *PSD* measurements or microscopy measurements, as described below.

### 3.3. *SBP* microgels (*SBPM*)

### 3.3.1. Characterisation of SBPM via microscopy

Fig. 5A shows a photograph of a typical free-standing *SBP* hydrogel prior to mechanical disruption. Microgel suspensions imaged via transmission optical microscopy are shown in Fig. 5B. Addition of crystal violet and concentration of the sample by mild centrifugation was found to improve the image quality (see section 2.2.6). Highly irregular shaped particles were observed for these microgels, made from  $C_{GEL} = 2.4$  wt.%, i.e., the weakest gel. Alginate-based microgels prepared by fragmenting calcium alginate (macro)gel beads in a commercial food processor were found to have a similar morphology when imaged with light microscopy (Yu, Jia, Cheng, Zhang, & Zhuo, 2010). This was also the case for calcium cross-linked *LMP* microgels fabricated by Saavedra Isusi et al. (2019) and the agarose microgels fabricated by Ellis and Jacquier (2009). On the other hand, polysaccharide microgel particles prepared by a similar top-down disruption of emulsion filled starch hydrogels of higher  $G'$  (ca.  $3 \times 10^3$  to  $6 \times 10^3$  Pa) showed a much more spherical structure whilst in the same size range (Torres, Tena, Murray, & Sarkar, 2017). The average size of the microgels also increased with increasing  $G'$  of the parent hydrogel. Since the cross-links in starch gels are based on non-covalent interactions, (i.e., hydrogen bonding), possibly the irregular shape of covalently cross-linked *SBPM* is a result of stronger cross-links, which likely lead to more random fracture of the hydrogel.

*CLSM* was also used to characterise the microgel samples and provided clear images of the irregular microgel particle structure, as the example in Fig. 5C shows. Many of the particles seemed to possess flat, smooth sides. Undoubtedly, the interfacial region is more diffuse than this suggests, but such structural features are expected to be well below the resolution of *CLSM*. Scanning electron micrographs of these microgel samples, shown in Fig. 5D, also seem to preserve this type of morphology, although the average size of the particles was somewhat smaller, with a significant proportion of micron and sub-micron sized particles. It is likely that this apparent difference in size range was a result of the various additional processing steps involved in the *SEM* analysis (see section 2.2.6). It should also be noted that the images in Fig. 5C and Fig. 5D were obtained from a different batch of *SBP* than Fig. 5B and using a Silverson blender to fragment the hydrogel (see Methods section 2.2.2) - although the final fitted value of  $G'_{inf}$  ( $224 \pm 2$  Pa, see Fig. S3) of the gel was almost identical to that in Fig. 5B ( $223 \pm 2$  Pa). A small fraction of particles in this lower size range is suggested in the light scattering measurements of the microgel dispersions made from gels of these  $G'_{inf}$  values - see next section below. No significant changes in microgel particle size with time were observed in any of the microscopy techniques used.

### 3.3.2 SBPM particle size distribution (PSD) via laser diffraction

Fig. 6 shows the *PSD* of *SBPM* obtained from parent hydrogels of different  $C_{GEL}$ . Table 3 shows the various parameters used to describe the resulting *PSDs*, alongside the corresponding hydrogel rheology data already discussed above. All microgel suspensions exhibited a *PSD* in which the main peak was between 10 and 100  $\mu\text{m}$ . There is some evidence for a bimodal particle size distribution in the microgels prepared from  $C_{GEL} = 2.4$  wt.%, in the form of a shoulder extending from the major peak to lower particle sizes and a smaller, discrete peak at around 1  $\mu\text{m}$ . It is worth noting that the *SEM* images for this particular sample (Fig. 5D) also suggested some particles in this lower size range. However, it is also plausible that this peak corresponds to some high molecular weight pectin species or their aggregates, e.g. enzymatically cross-linked pectin components incompletely incorporated into the bulk gel, or liberated from the bulk hydrogel during its comminution. Drying of the pellet and supernatant and comparing this with the known original mass of pectin gel in the sample suggested that if this was the case, these elements represented a minute fraction (e.g., < 1 %) of the total pectin in the system. It has been shown elsewhere that, a more extensive cross-linking in *SBP* hydrogels resulted in a reduced sol fraction and thus a greater yield of cross-linked material (Micard, et al., 1999; Robertson, Faulds, Smith, & Waldron, 2008). Note that this lower size fraction was only exhibited in the *PSDs* for the microgels prepared from the lowest  $C_{GEL} = 2.4$  wt.% and results in a broadening of the *Span* relative to the (monomodal) *PSDs* for the two stronger hydrogels (see Table 3). However, caution should be used in interpreting the *PSDs* since they are calculated *via* Mie theory, which assumes spherical particles, whilst Fig. 5 clearly indicates that this is not the case. Notwithstanding these provisos, Table 3 suggests that there is a clear trend for larger particle sizes at the higher  $C_{GEL}$  and therefore at the higher the  $G'_{inf}$ , i.e., 4 wt.% > 3.4 wt.% > 2.4 wt.%. This suggests that the tougher microgels are harder to break down using the shear procedures employed. We note that Saavedra Isusi et al. (2019), using a combination of rotor-stator mixing and wet milling, obtained smaller *LMP* microgels from hydrogels with higher elastic moduli but that had lower yield stresses and strains and the shortest LVER-region. On the other hand, Ellis and Jacquier (2009) found that the average size of agarose microgels increased with increasing polymer concentration in the range 1 to 3 wt.% agarose, but between 4 and 8 wt.% agarose the mean particle size was approximately the same ( $D_{32} \approx 100 \mu\text{m}$ ). The authors suggested that this was because, at 3 wt.% agarose and above, the gel yield strain (measured *via* compression) was approximately the same. Torres et al. (2107) also found that there was a positive correlation between the yield strain (measured *via* shear rheometry) of their starch-based hydrogels and a larger mean size of the

microgels produced from them. Unfortunately, it is hard to measure or calculate the actual shear stresses and strains applied to the gels in a blender or homogenizer.

A limited number of oscillatory shear amplitude sweeps were performed on *quiescently* developed hydrogels at a frequency of 1 Hz, shown in Supplementary Fig. S4. Before commencing the measurements the gels were allowed to develop for 2 h for  $C_{GEL} = 2.4$  wt.% and for 4 h for  $C_{GEL} = 3.4$  and 4 wt.% SBP, i.e., the gels were close to achieving their maximum value of  $G'$ . All 3 gels showed some strain hardening, followed by a sharp decrease in  $G'$  (and increase in  $G''$ ) above a particular strain, i.e., they started to yield. Arbitrarily taking the yield strain ( $\gamma_y$ ) and stress ( $\sigma_y$ ) as the values where the maximum in  $G'$  occurred, these values were: 84% and 460 Pa for  $C_{GEL} = 2.4$  wt.%, 63% and 747 Pa for  $C_{GEL} = 3.4$  wt.%; 63 % and 853 Pa for  $C_{GEL} = 4$  wt.%. With more detailed measurements it would be possible to pinpoint the maximum in  $G'$  and therefore  $\gamma_y$  more accurately, but essentially it is seen that there is the same correlation between larger particle sizes and higher  $\sigma_y$  as with higher  $G'_{inf}$ , discussed above. For  $C_{GEL} = 3.4$  wt.% and 4 wt.% no difference in  $\gamma_y$  was observed, but for the weakest gel, i.e.,  $C_{GEL} = 3.4$  wt.%,  $\gamma_y$  was slightly higher, i.e., this gel is slightly less brittle.

Finally, it was demonstrated that the *SBPM* seemed perfectly stable to pasteurization-type conditions, at least as far as their *PSD* was concerned. A sample of *SBPM* ( $C_{GEL} = 3.4$  wt.%) was heated at 85°C for 1 h then cooled to room temperature before re-sizing. There was negligible difference between the *PSDs* before and after the heating procedure (see Supplementary Fig. S5)

### 3.4 Rheology of *SBPM* dispersions

A potential application of biopolymer microgels is their use as rheology modifiers in foods. The bulk rheology for such systems is expected to be mainly dependent on the particle volume fraction ( $\phi$ ) and shape, though the particle deformability and the potential for inter-penetration will also be important at high  $\phi$ . Characterization of the effective  $\phi$  of microgels requires detailed measurements and modelling at a wide range of microgel concentrations and is not the purpose of this current work (although it is the subject of our ongoing investigations). Instead, we wish to highlight the potential of these *stable SBPM* for controlling rheological properties.

Fig. 7 shows viscosity ( $\eta$ ) curves as a function of shear stress ( $\sigma$ ) for the *SBPM* suspensions ( $C_{GEL} = 2.4$  wt.% *SBP*). We describe the systems in terms of the wt.% of particles ( $C_{MG}$ ) as well as the total wt.% of pectin  $C_{PTOTAL}$  in the system, in order to make comparisons with  $\eta$  of native (i.e., non-gelled) *SBP*

solutions. The *SBP* solutions showed pronounced pseudoplasticity, with the shear thinning region separated by lower and upper Newtonian plateaus in  $\eta$ . Such behaviour is well known and corresponds to the progressive disentanglement of polymer chains with increasing shear rate ( $\dot{\gamma}$ ) or shear stress ( $\sigma$ ). The stretching and alignment of polymer molecules in the direction of the shear reduces the resistance to flow and thus reduces  $\eta$  (Lapasin & Prici, 1995). Profound differences were observed in the flow properties of the microgel suspensions when compared to *SBP* solutions at similar  $C_{PTOTAL}$ . Most striking is the massive increase in the zero shear viscosity ( $\eta_0$ ) at relatively higher  $\sigma$ . The microgel dispersions of  $C_{PTOTAL} = 0.8$  wt.% gave  $\eta_0$  of the order of  $2.3 \times 10^4$  Pa s. In comparison, native *SBP* solutions prepared at more than double this overall polymer concentration, i.e. the sample with  $C_{PTOTAL} = 1.7$  wt.%, gave an apparent  $\eta_0$  of only 44 Pa s.

Pseudoplasticity was observed at all  $C_{MG}$  but the mechanism is likely to be more complex than the shear thinning behaviour in biopolymer solutions, given that microgels are a hybrid system between a particle and a high MW branched polymer molecule. The viscosity curves of the microgel suspensions are more akin to those of so-called 'structured fluids' that demonstrate a clear yield stress ( $\sigma_y$ ). The  $\eta_0$  Newtonian plateau is attributed to creeping flow of the suspensions until a critical stress is reached (i.e.  $\sigma_y$ ), at which point the suspensions yield strongly and begin to flow, as characterised by a decrease in  $\eta$  by several orders of magnitude over a narrow range of  $\sigma$  (Barnes, 1999).

Viscosity curves for microgel suspensions were performed in triplicate using a new sample loading for each and it is worth mentioning that the  $\eta$  versus  $\sigma$  curves were, within experimental error, completely reversible on repeating the measurement on the same sample. Fig. S6 also demonstrates this, for a sample at  $C_{PTOTAL} = 1.1$  wt.%,  $C_{GEL} = 3.4$  % *SBP*, where repeated measurement cycles on the same sample but at decreasing gap widths overlap almost perfectly. (This test also suggest that any wall slip was negligible). The error in the measurements was always largest in the region of greatest shear thinning, which by analogy to structured fluids is where the microstructure is most greatly disrupted. Future work, to determine an effective  $\phi$  for these microgel dispersions and an investigation of any time-dependent rheological properties will allow us to determine whether such systems behave as 'soft glassy materials' or 'particulate gels'.

Another interesting feature of the data in Figure 7 is that, despite their 'solid-like' behaviour at low  $\sigma$ , in the range of high  $\sigma$  ( $> 10$  Pa), the microgel suspensions appeared to be still shear thinning and heading for lower  $\eta$  than that of the *SBP* solutions studied. This phenomenon might be a further

advantage of *SBPM* over *SBP* (or other polysaccharide) solutions as thickeners, when material has to be mixed, pumped, deposited, etc., at very high shear rates. The highest  $\sigma$  applied to the microgel suspensions (sample with  $C_{PTOTAL} = 0.8$  wt.%) corresponds to a  $\dot{\gamma}$  of approximately  $1000 \text{ s}^{-1}$ , which seemed to be around the maximum accessible  $\dot{\gamma}$  before the microgel samples were ejected from the gap. Therefore, it was not possible to locate a high shear limiting  $\eta$  for the microgel systems. It is possible that the soft microgel particles may change their shape at high shear, or that water may be squeezed out of them, both of which may result in extra contributions to a reduction in  $\eta$ .

The ULTRA-TURRAX rotor-stator type apparatus is a much simpler method of creating *SBPM* than two-stage homogenization, likely to be available much more generally and was seen to generate stable microgel particles with interesting rheological properties. However, in future work we also intend to put such *SBP* gel material through the sort of two stage blender + homogenizer process as initially tested on the LMP-Ca<sup>2+</sup> hydrogels, to see if this generates different sized particles and/or particles with significantly different bulk rheology at equivalent concentrations of the particle sizes studied here. With the *LMP*, this seemed to increase microgel dissolution in water, whereas the *SBPM* seem to be perfectly stable in water. Certainly, if the *SBPM* particles are surface active, in order to stabilise micron sized emulsion droplets, the stabilizing *SBPM* will have to be smaller than those studied here.

#### 4. Conclusions

The mechanical disruption of hydrogels in the presence of excess solvent has proven to be a simple and scalable technique to produce microgel suspensions from physically and chemically cross-linked pectin hydrogels. For the former, we have shown how the stability of *LMP* based microgel particles to dissolution can be improved if calcium ions remain in the dispersion medium. However, much more robust polysaccharide-based microgels can be produced from covalently cross-linked *SBP* hydrogels. The latter are of interest for industrial food processing applications because they are resistant to dissolution on prolonged storage in contact with water and can provide a much wider range of viscosities than just solutions of pectin at similar overall pectin concentrations. Furthermore, *SBP* gels cross-linked by laccase are thermally irreversible (Khalighi, Berger, & Ersoy, 2020). The same seems to be true for the *SBPM* particles (fig. S5), which will be a clear advantage over other microgel particles, that might dissipate during pasteurization in food applications.

Light scattering measurements suggest that the size (1 to 100  $\mu\text{m}$ ) of *SBPM* can be tailored *via* the mechanical properties of the parent hydrogels, which depend strongly on polymer concentration: stronger *SBP* hydrogels lead to larger *SBPM*. Microscopy across a range of techniques and magnifications suggested that the microgels consist of highly irregularly shaped particles. Dispersions of between 37 and 50 wt.% *SBPM* (equivalent to 0.6 and 0.8 wt.% pectin) were highly pseudoplastic with very high (approximately 500 to 20,000 Pa s) low shear rate limiting viscosities, but extremely shear thinning with increasing shear stress, with no apparent limiting viscosity up to shear rates of approximately  $1000\text{ s}^{-1}$  (the practical limit of measurement). Future work is required to understand the rheology of the *SBPM* systems in more detail, in terms of their effective volume fraction, particle deformability and particle interactions. In addition, we hope to demonstrate their use as rheology modifiers and emulsifiers in more complex systems, closer to real foods.

## 5. Acknowledgements

Authors gratefully acknowledge the Engineering and Physical Sciences Research Council (EPSRC) funded Centre for Doctoral Training in Soft Matter and Functional Interfaces (SOFI), Grant Ref. No. EP/L015536/1 as well as Nestlé PTC Confectionery (York, UK) for financial support. We also acknowledge excellent technical support from Mark Ambühl and Carine Morgenegg (Imaging Group, Nestle Research Center, Vers-chez-les-Blanc, Switzerland) in obtaining the SEM images.

## 6. References

- Allan-Wojtas, P., & Kalab, M. (1984). A simple procedure for preparation of stirred yoghurt for scanning electron microscopy. *Food Microstructure*, 3, 197-198.
- Barnes, H. (1999). The yield stress a review or 'panta roi' everything flows? In.
- Berth, G., Dautzenberg, H., & Hartmann, J. (1994). Static light scattering technique applied to pectin in dilute solution. Part III: The tendency for association. *Carbohydrate Polymers*, 25(3), 197-202.
- Braccini, I., & Pérez, S. (2001). Molecular Basis of  $\text{Ca}^{2+}$ -Induced Gelation in Alginates and Pectins: The Egg-Box Model Revisited. *Biomacromolecules*, 2(4), 1089-1096.
- Bunzel, M. (2010). Chemistry and occurrence of hydroxycinnamate oligomers. *Phytochemistry Reviews*, 9(1), 47-64.
- Burey, P., Bhandari, B. R., Howes, T., & Gidley, M. J. (2008). Hydrocolloid Gel Particles: Formation, Characterization, and Application. *Critical Reviews in Food Science and Nutrition*, 48(5), 361-377.
- Cao, Y., & Mezzenga, R. (2020). Design principles of food gels. *Nature Food*, 1(2), 106-118.
- Cheng, K., & Lim, L. Y. (2004). Insulin-Loaded Calcium Pectinate Nanoparticles: Effects of Pectin Molecular Weight and Formulation pH. *Drug Development and Industrial Pharmacy*, 30(4), 359-367.

- Colquhoun, I. J., Ralet, M.-C., Thibault, J.-F., Faulds, C. B., & Williamson, G. (1994). Structure identification of feruloylated oligosaccharides from sugar-beet pulp by NMR spectroscopy. *Carbohydrate Research*, *263*(2), 243-256.
- Dickinson, E. (2017). Biopolymer-based particles as stabilizing agents for emulsions and foams. *Food Hydrocolloids*, *68*, 219-231.
- Djabourov, M., Nishinari, K., & Ross-Murphy, S. B. (2013). 4. General Properties of Polymer Networks. In *Physical Gels from Biological and Synthetic Polymers*: Cambridge University Press.
- Ellis, A., & Jacquier, J. C. (2009). Manufacture and characterisation of agarose microparticles. *Journal of Food Engineering*, *90*(2), 141-145.
- Farjami, T., & Madadlou, A. (2017). Fabrication methods of biopolymeric microgels and microgel-based hydrogels. *Food Hydrocolloids*, *62*, 262-272.
- Fernández Farrés, I., & Norton, I. T. (2014). Formation kinetics and rheology of alginate fluid gels produced by in-situ calcium release. *Food Hydrocolloids*, *40*, 76-84.
- Gombotz, W. R., & Wee, S. (1998). Protein release from alginate matrices. *Advanced Drug Delivery Reviews*, *31*(3), 267-285.
- Gosal, W. S., Clark, A. H., & Ross-Murphy, S. B. (2004). Fibrillar  $\beta$ -Lactoglobulin Gels: Part 2. Dynamic Mechanical Characterization of Heat-Set Systems. *Biomacromolecules*, *5*(6), 2420-2429.
- Grant, G. T., Morris, E. R., Rees, D. A., Smith, P. J. C., & Thom, D. (1973). Biological interactions between polysaccharides and divalent cations: The egg-box model. *FEBS Letters*, *32*(1), 195-198.
- Guillon, F., & Thibault, J.-F. (1987). Characterization and oxidative cross-linking of sugar beet pectins after mild acid hydrolysis and arabanases and galactanases degradation. *Food Hydrocolloids*, *1*(5), 547-549.
- Guillon, F., & Thibault, J.-F. (1990). Oxidative cross-linking of chemically and enzymatically modified sugar-beet pectin. *Carbohydrate Polymers*, *12*(4), 353-374.
- Guillon, F., Thibault, J.-F., Rombouts, F., Voragen, A. G. J., & Pilnik, W. (1989). Enzymic hydrolysis of the "hairy" fragments of sugar-beet pectins. *Carbohydrate Research*, *190*(1), 97-108.
- Guo, J., Zhou, Q., Liu, Y.-C., Yang, X.-Q., Wang, J.-M., Yin, S.-W., & Qi, J.-R. (2016). Preparation of soy protein-based microgel particles using a hydrogel homogenizing strategy and their interfacial properties. *Food Hydrocolloids*, *58*, 324-334.
- Ishii, T., & Matsunaga, T. (1996). Isolation and characterization of a boron-rhamnogalacturonan-II complex from cell walls of sugar beet pulp. *Carbohydrate Research*, *284*(1), 1-9.
- Jiao, B., Shi, A., Wang, Q., & Binks, B. P. (2018). High-Internal-Phase Pickering Emulsions Stabilized Solely by Peanut-Protein-Isolate Microgel Particles with Multiple Potential Applications. *Angewandte Chemie International Edition*, *57*(30), 9274-9278.
- Joye, I. J., & McClements, D. J. (2014). Biopolymer-based nanoparticles and microparticles: Fabrication, characterization, and application. *Current Opinion in Colloid & Interface Science*, *19*(5), 417-427.
- Kalab, M. (1988). Encapsulation of viscous food in agar gel tubes for electron microscopy. *Food Microstructure*, *7*, 213-214.
- Khalighi, S., Berger, R. G., & Ersoy, F. (2020). Cross-Linking of Fibrex Gel by Fungal Laccase: Gel Rheological and Structural Characteristics. *Processes*, *8*(1), 16.
- Kuuva, T., Lantto, R., Reinikainen, T., Buchert, J., & Autio, K. (2003). Rheological properties of laccase-induced sugar beet pectin gels. *Food Hydrocolloids*, *17*(5), 679-684.
- Lapasin, R., & Prici, S. (1995). Rheology of polysaccharide systems. In *Rheology of Industrial Polysaccharides: Theory and Application* (First edition ed.). Glasgow, UK: Blackie Academic and Professional.
- Loveday, S. M., Su, J., Rao, M. A., Anema, S. G., & Singh, H. (2011). Effect of Calcium on the Morphology and Functionality of Whey Protein Nanofibrils. *Biomacromolecules*, *12*(10), 3780-3788.

- Luzio, G. A., & Cameron, R. G. (2008). Demethylation of a model homogalacturonan with the salt-independent pectin methyltransferase from citrus: Part II. Structure–function analysis. *Carbohydrate Polymers*, *71*(2), 300-309.
- Matsumiya, K., & Murray, B. S. (2016). Soybean protein isolate gel particles as foaming and emulsifying agents. *Food Hydrocolloids*, *60*, 206-215.
- Matthew, J. A., Howson, S. J., Keenan, M. H. J., & Belton, P. S. (1990). Improvement of the gelation properties of sugarbeet pectin following treatment with an enzyme preparation derived from *Aspergillus niger* — Comparison with a chemical modification. *Carbohydrate Polymers*, *12*(3), 295-306.
- May, C. D. (1990). Industrial pectins: Sources, production and applications. *Carbohydrate Polymers*, *12*(1), 79-99.
- McClements, D. J. (2017). Designing biopolymer microgels to encapsulate, protect and deliver bioactive components: Physicochemical aspects. *Advances in Colloid and Interface Science*, *240*, 31-59.
- Micard, V., & Thibault, J.-F. (1999). Oxidative gelation of sugar-beet pectins: use of laccases and hydration properties of the cross-linked pectins. *Carbohydrate Polymers*, *39*(3), 265-273.
- Murray, B. S. (2019). Microgels at fluid-fluid interfaces for food and drinks. *Advances in Colloid and Interface Science*, *271*, 101990.
- Nikolova, K., Panchev, I., & Sainov, S. (2007). Van der Waals parameters, refractive indices and dispersion equation of pectin. *Journal of Optoelectronics and Advanced Materials*, *9*(2), 468.
- Norsker, M., Jensen, M., & Adler-Nissen, J. (2000). Enzymatic gelation of sugar beet pectin in food products. *Food Hydrocolloids*, *14*(3), 237-243.
- Oosterveld, A., Beldman, G., Searle-van Leeuwen, M. J. F., & Voragen, A. G. J. (2000). Effect of enzymatic deacetylation on gelation of sugar beet pectin in the presence of calcium. *Carbohydrate Polymers*, *43*(3), 249-256.
- Oosterveld, A., Beldman, G., & Voragen, A. G. J. (2000). Oxidative cross-linking of pectic polysaccharides from sugar beet pulp. *Carbohydrate Research*, *328*(2), 199-207.
- Pelton, R., & Hoare, T. (2011). Microgels and Their Synthesis: An Introduction. In A. Fernandez-Nieves, H. Wyss, J. Mattsson & D. Weitz (Eds.), *Microgel Suspensions* (pp. 1-32). Germany: Wiley-VCH.
- Peppas, N. A. (1991). Physiologically Responsive Hydrogels. *Journal of Bioactive and Compatible Polymers*, *6*(3), 241-246.
- Pippen, E. L., McCready, R. M., & Owens, H. S. (1950). Gelation Properties of Partially Acetylated Pectins. *Journal of the American Chemical Society*, *72*(2), 813-816.
- Ralet, M.-C., Cabrera, J. C., Bonnin, E., Quémener, B., Hellin, P., & Thibault, J.-F. (2005). Mapping sugar beet pectin acetylation pattern. *Phytochemistry*, *66*(15), 1832-1843.
- Renard, C. M. G. C., Crépeau, M.-J., & Thibault, J.-F. (1995). Structure of the repeating units in the rhamnogalacturonic backbone of apple, beet and citrus pectins. *Carbohydrate Research*, *275*(1), 155-165.
- Robertson, J. A., Faulds, C. B., Smith, A. C., & Waldron, K. W. (2008). Peroxidase-Mediated Oxidative Cross-Linking and Its Potential To Modify Mechanical Properties in Water-Soluble Polysaccharide Extracts and Cereal Grain Residues. *Journal of Agricultural and Food Chemistry*, *56*(5), 1720-1726.
- Ross-Murphy, S. B. (1995). Rheological Characterisation of Gels. *Journal of Texture Studies*, *26*(4), 391-400.
- Saavedra Isusi, G. I., Karbstein, H. P., & van der Schaaf, U. S. (2019). Microgel particle formation: Influence of mechanical properties of pectin-based gels on microgel particle size distribution. *Food Hydrocolloids*, *94*, 105-113.
- Sarkar, A., Murray, B., Holmes, M., Ettelaie, R., Abdalla, A., & Yang, X. (2016). In vitro digestion of Pickering emulsions stabilized by soft whey protein microgel particles: influence of thermal treatment. *Soft Matter*, *12*(15), 3558-3569.

- Shewan, H. M., & Stokes, J. R. (2013). Review of techniques to manufacture micro-hydrogel particles for the food industry and their applications. *Journal of Food Engineering*, 119(4), 781-792.
- Shewan, H. M., Stokes, J. R., & Smyth, H. E. (2020). Influence of particle modulus (softness) and matrix rheology on the sensory experience of 'grittiness' and 'smoothness'. *Food Hydrocolloids*, 103, 105662.
- Smith, J. E., & Stainsby, G. (1977). Studies on pectins I. Light-scattering and MW. *British Polymer Journal*, 9(4), 284-289.
- Sorochan, V. D., Dzizenko, A. K., Bodin, N. S., & Ovodov, Y. S. (1971). Light-scattering studies of pectic substances in aqueous solution. *Carbohydrate Research*, 20(2), 243-249.
- Sriamornsak, P., & Kennedy, R. A. (2008). Swelling and diffusion studies of calcium polysaccharide gels intended for film coating. *International Journal of Pharmaceutics*, 358(1), 205-213.
- Stokes, J. R. (2011). Rheology of Industrially Relevant Microgels. In A. Fernandez-Nieves, H. Wyss, J. Mattsson & D. Weitz (Eds.), *Microgel Suspensions* (pp. 327-353). Weinheim, Germany: Wiley-VCH.
- Thibault, J. F., Garreau, C., & Durand, D. (1987). Kinetics and mechanism of the reaction of ammonium persulfate with ferulic acid and sugar-beet pectins. *Carbohydrate Research*, 163(1), 15-27.
- Thibault, J. F., & Rombouts, F. M. (1986). Effects of some oxidising agents, especially ammonium peroxy sulfate, on sugar-beet pectins. *Carbohydrate Research*, 154(1), 205-215.
- Torres, O., Tena, N. M., Murray, B., & Sarkar, A. (2017). Novel starch based emulsion gels and emulsion microgel particles: Design, structure and rheology. *Carbohydrate Polymers*, 178, 86-94.
- Williamson, G., Faulds, C. B., Matthew, J. A., Archer, D. B., Morris, V. J., Brownsey, G. J., & Ridout, M. J. (1990). Gelation of sugarbeet and citrus pectins using enzymes extracted from orange peel. *Carbohydrate Polymers*, 13(4), 387-397.
- Yu, C.-Y., Jia, L.-H., Cheng, S.-X., Zhang, X.-Z., & Zhuo, R.-X. (2010). Fabrication of microparticle protein delivery systems based on calcium alginate. *Journal of Microencapsulation*, 27(2), 171-177.
- Zaidel, D. N. A., Chronakis, I. S., & Meyer, A. S. (2012). Enzyme catalyzed oxidative gelation of sugar beet pectin: Kinetics and rheology. *Food Hydrocolloids*, 28(1), 130-140.
- Zhang, S., Holmes, M., Ettelaie, R., & Sarkar, A. (2020). Pea protein microgel particles as Pickering stabilisers of oil-in-water emulsions: Responsiveness to pH and ionic strength. *Food Hydrocolloids*, 102, 105583.

## Tables and Figures

**Table 1.** Degree of methoxylation ( $DM$ ), degree of acetylation ( $D_{AC}$ ), degree of amidation ( $D_{AM}$ ) and molecular weight ( $M_W$ ) of *LMP* and *SBP*, as specified by the manufacturer

Pectin Type	$DM$ / %	$D_{AC}$ / %	$D_{AM}$ (%)	$M_W$ (kDa)
GENU LM-104 AS	27	-	20	$89.1 \pm 3.1^a$
GENU BETA	55	14 - 26	-	> 60

<sup>a</sup> – Viscosity average MW determined by (Cheng & Lim, 2004)

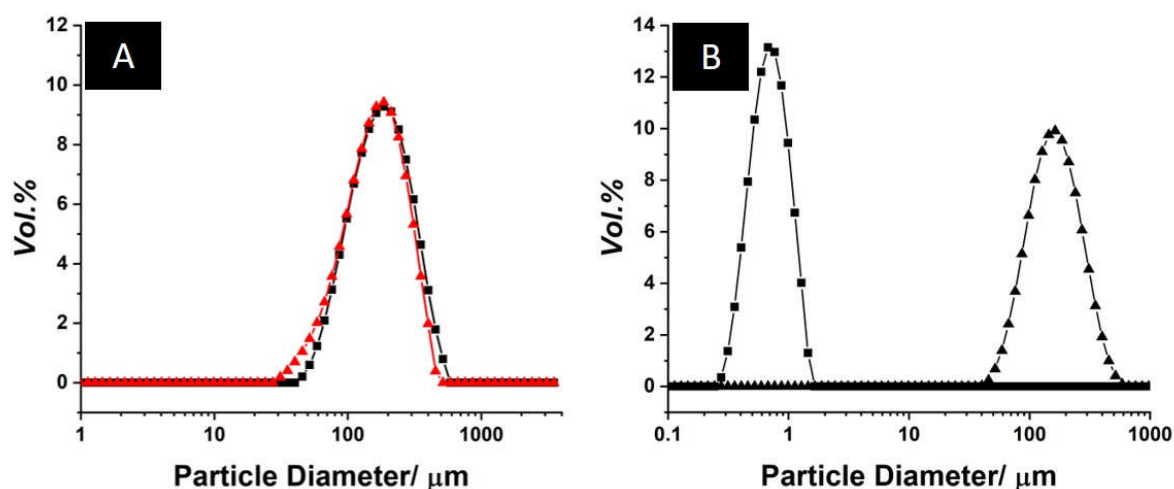


**Fig. 1.** Particle size distributions obtained from laser diffraction for *LMP* microgels physically cross-linked *via* 8.34 mM  $Ca^{2+}$ . (A) Prepared *via* UltraTurrax in 8.34 mM  $CaCl_2$ , dispersed in Mastersizer tank (in water) and measured after 1 min (■) and 60 min (■). (B) Prepared *via* UltraTurrax and Jet Homogenizer in Milli-Q water (■) or 8.34 mM  $CaCl_2$  (▲), dispersed in Mastersizer tank (in water) and measured after 1 min.

**Table 2.** Particle size distribution measures obtained from laser diffraction measurements of *LMP* microgels formed from bulk hydrogels cross-linked *via* 8.34 mM  $CaCl_2$ .

Dispersion method	Dispersion medium during microgel formation	Time in Mastersizer tank/ min	$D_{3,2}$ / $\mu m$	$D_{4,3}$ / $\mu m$	$D_{90}$ / $\mu m$	Span	Residuals / %
UltraTurrax only	8.34 mM $CaCl_2$	1	163	209	355	1.39	0.8
UltraTurrax only	8.34 mM $CaCl_2$	60	143	188	319	1.38	0.9
Silverson + valve homogenizer	Milli-Q water	1	0.69	0.78	1.17	0.963	32.4
Silverson + valve homogenizer	8.34 mM $CaCl_2$	1	151	190	319	1.354	0.7

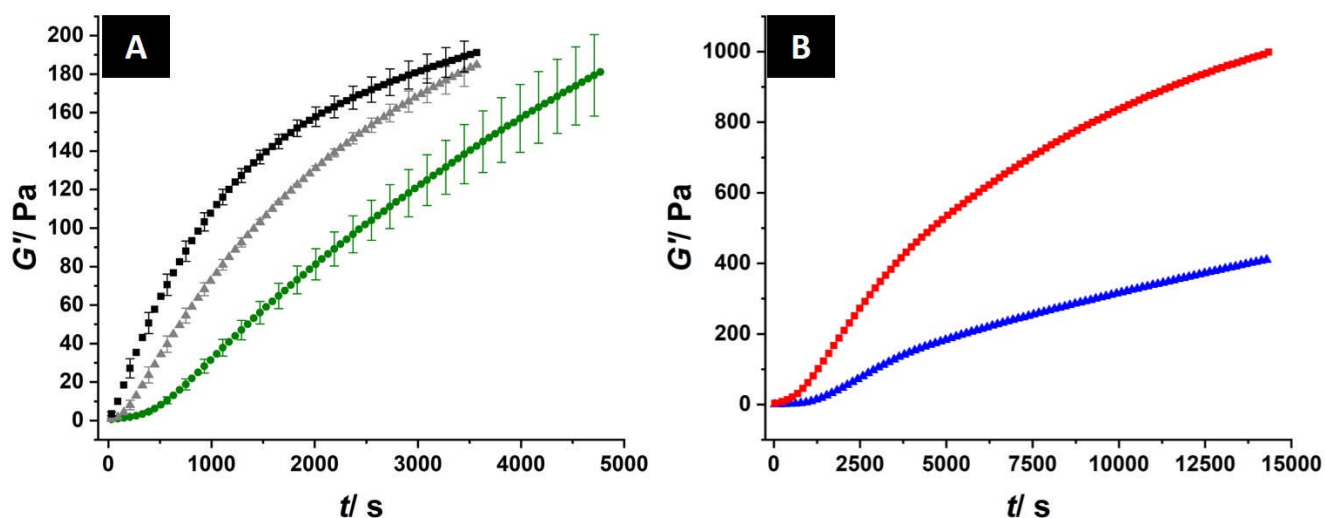


**Fig. 2.** (A) Evolution of  $G'$  with time for *SBP* hydrogels prepared with  $C_{GEL} = 2.4$  wt.% *SBP* plus  $C_E = 0.1$  ( $\bullet$ ),  $0.2$  ( $\blacktriangle$ ) and  $0.4$  ( $\blacksquare$ )  $\text{mg ml}^{-1}$  laccase. Mean values are shown for 3 separate measurements. For clarity, only every third data point is plotted and error bars (standard deviations) for every two of these data points. (B) Evolution of  $G'$  with time for *SBP* hydrogels prepared with  $C_{GEL} = 3.4$  ( $\blacktriangle$ ) and ( $\blacksquare$ )  $4$  wt.% *SBP* plus  $C_E = 0.1$   $\text{mg ml}^{-1}$  laccase. Every 5<sup>th</sup> data point is plotted.

**Table 3:** Fitted equilibrium dynamic storage moduli ( $G'_{inf}$ ) and kinetic constant  $B$ , according to equation (3) (see Figure S2) for the evolution of *SBP* hydrogels at various *SBP* concentrations ( $C_{GEL}$ ) and laccase concentrations ( $C_E$ ).  $R^2$  = mean regression coefficient. Also shown are the average particle sizes ( $D_{3,2}$ ,  $D_{4,3}$ ) and *Span* values determined by laser diffraction for the corresponding microgels obtained from these hydrogels.

Concentrations		<i>SBP</i> hydrogels			<i>SBP</i> microgels		
$C_{GEL}/$ wt.%	$C_E/$ $\text{mg ml}^{-1}$	$*G'_{inf}/$ Pa	$*B/$ s	$R^2$	$D_{3,2}/$ $\mu\text{m}$	$D_{4,3}/$ $\mu\text{m}$	<i>Span</i>
2.4	0.4	$223 \pm 2$	$677 \pm 13$	0.9872	-	-	-
2.4	0.2	$250 \pm 3$	$1226 \pm 21$	0.9898	-	-	-
2.4	0.1	$293 \pm 3$	$2515 \pm 32$	0.9929	16	32	1.78
3.4	0.1	$573 \pm 3$	$5662 \pm 47$	0.9908	37	44	1.14
4	0.1	$1286 \pm 5$	$4230 \pm 32$	0.9918	50	58	1.06

\* $P < 0.0001$  in all cases.  $\pm$  values are standard errors

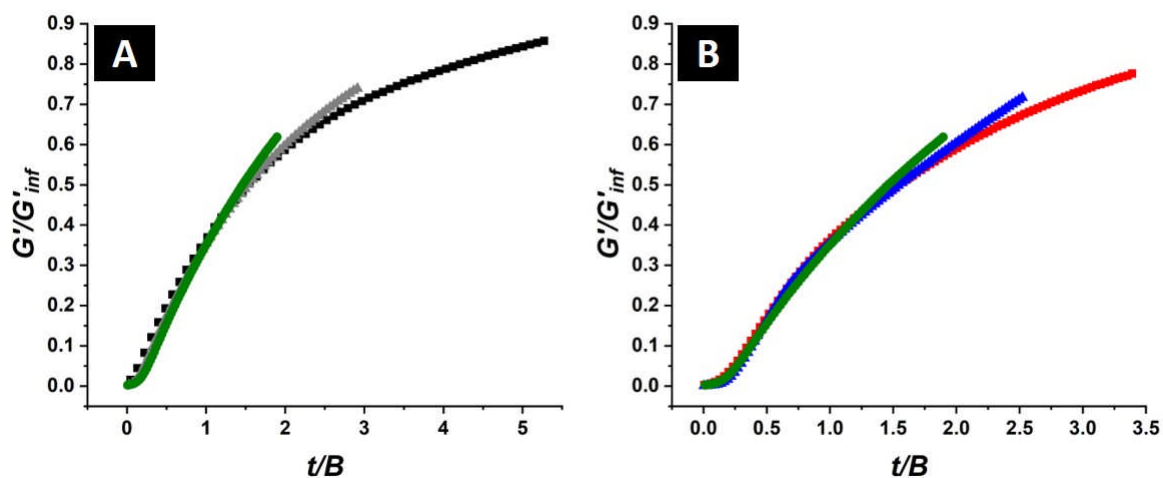


**Fig. 3.** Scaled plots of  $G'/G'_{inf}$  versus reduced time  $t/B$  for the data shown in Figure 2. (A) Hydrogels prepared with  $C_{GEL} = 2.4$  wt.% SBP plus  $C_E = 0.1$  (●), 0.2 (▲) and 0.4 (■) mg ml<sup>-1</sup> laccase. (B) Hydrogels prepared with  $C_{GEL} = 2.4$  (●), 3.4 (▲) and 4 (■) wt.% SBP plus  $C_E = 0.1$  mg ml<sup>-1</sup> laccase.

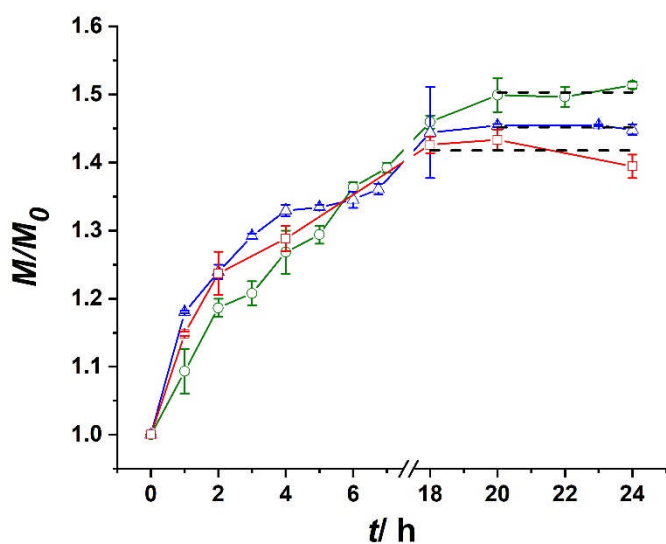


**Fig. 4.** Swelling experiments performed on SBP hydrogels prepared with  $C_{GEL} = 2.4$  (●), 3.4 (▲) and 4 (■) wt.% SBP plus 0.1 mg ml<sup>-1</sup> laccase. The mass of the hydrogels relative to their initial mass ( $M/M_0$ ) is plotted versus time ( $t$ ) immersed in deionized water (at pH 6). The solid lines are to guide the eye and the error bars correspond to the standard deviation based on a minimum of two

separate experiments. The dashed horizontal lines show the averages of the final three data points in each case, used to estimate of the final swelling ratio  $S$  (see text).

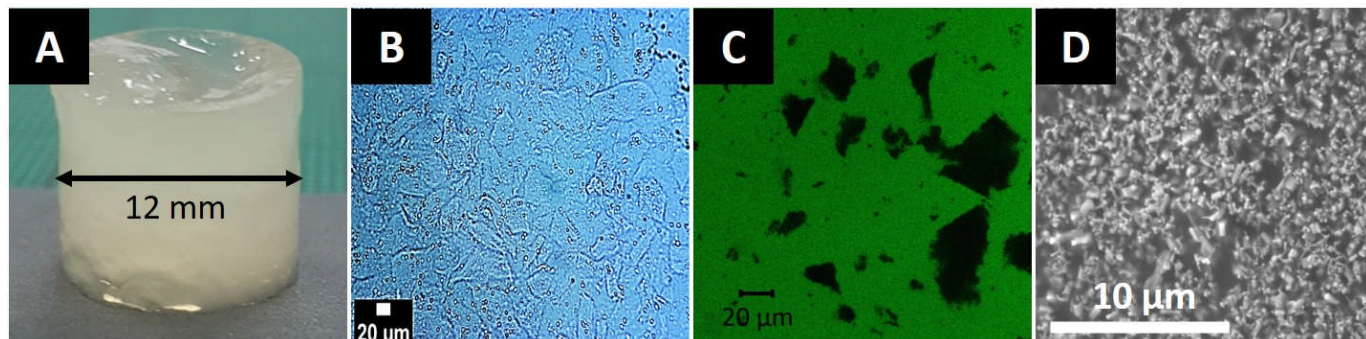


**Fig. 5.** (A) Photograph of a cylinder of *SBP* hydrogel prior to mechanical disruption. (B) Light microscopy image of *SBP* microgels stained by crystal violet. (C) CLSM image of *SBP* microgels: microgel particles appear black due to negative staining of the aqueous phase with FITC-dextran (green). (D) SEM micrograph of *SBP* microgels. Scale bars in B & C = 20  $\mu\text{m}$ , scale bar in D = 10  $\mu\text{m}$ .

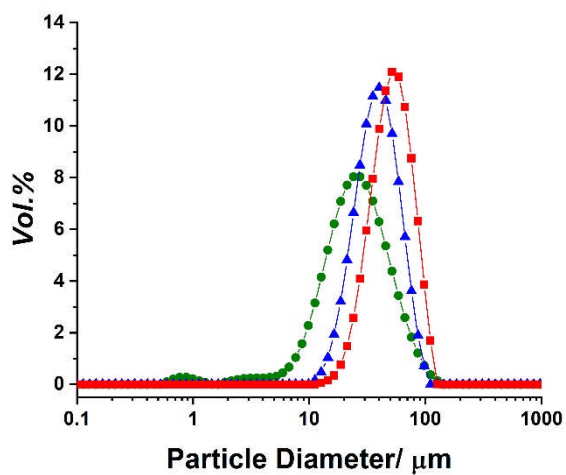


**Fig. 6.** Particle size distributions, as measured by laser diffraction of *SBP* microgels obtained from parent hydrogels prepared with  $C_{GEL} = 2.4$  ( $\bullet$ ), 3.4 ( $\blacktriangle$ ) and 4 ( $\blacksquare$ ) wt.% *SBP* plus  $0.1 \text{ mg ml}^{-1}$  laccase.

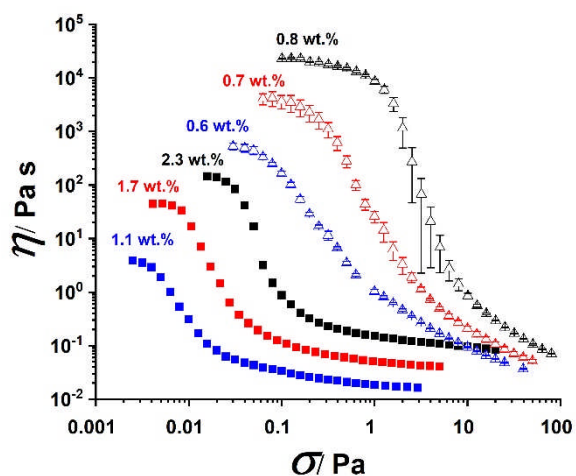


**Fig. 7.** Apparent viscosity ( $\eta$ ) as a function of shear stress ( $\sigma$ ) for native *SBP* solutions (filled symbols) at  $C_{PTOTAL} = 1.1$  wt.% (■), 1.7 wt.% (■) and 2.3 wt.% (■) and *SBP* microgel suspensions (open symbols) at  $C_{PTOTAL} = 0.6$  wt.% (△), 0.7 wt.% (△) and 0.8 wt.% (△), corresponding to  $C_{MG} = 37.6$ , 43.8 and 50.1 wt.%, respectively. The labels on the curves refer to the  $C_{PTOTAL}$  values. The microgel suspensions were obtained from parent hydrogels prepared with  $C_{GEL} = 2.4$  wt.% *SBP* plus  $0.1 \text{ mg ml}^{-1}$  laccase and concentrated to the specified  $C_{MG}$  by mild centrifugation and appropriate dilution with water. Measurements on microgel suspensions were performed in triplicate using a newly loaded sample for each and error bars = standard deviations. Viscosity curves for *SBP* solutions are based on one measurement.

## Supplementary Material

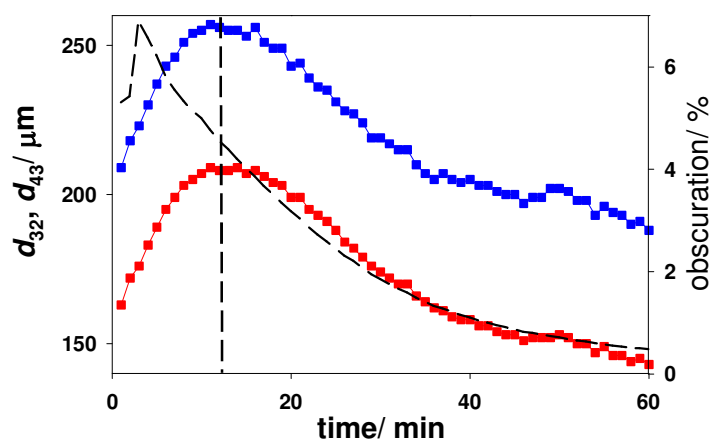


**Fig. S1.** Values of  $d_{32}$  (■) and  $d_{43}$  (■) as function of time, when measuring the size of *LMP* microgels created via the ULTRA-TURRAX in the presence of 8.34 mM  $\text{CaCl}_2$  and then dispersed in water in the Mastersizer tank. Also shown is the corresponding change in the % laser obscuration (dashed curved line) with time. Each individual measurement took 1 min. The changes to the left of the vertical dashed line are assumed to represent swelling of the *MGs*; to the right, their dissolution.

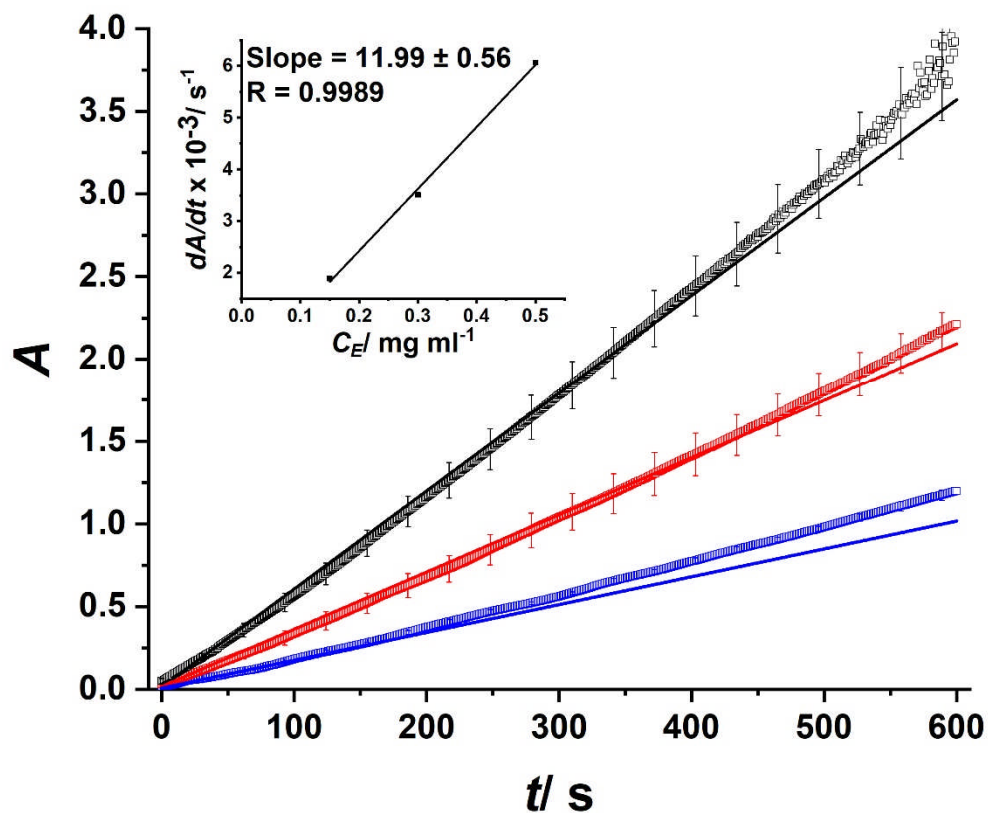


**Fig. S2.** Absorbance ( $A$ ) vs. time ( $t$ ) for the assay of enzyme activity measured *via* oxidation of ABTS at  $\lambda = 420$  nm, for Laccase Y120 enzyme at nominal enzyme concentrations  $C_E = 0.15$  (■),  $0.3$  (■) and  $0.5$  (■) mg ml<sup>-1</sup>. The inset shows the initial rate of ABTS oxidation ( $dA/dt$ ) determined from the gradient of the straight line fit to the data in the first 300 s. Error bars = standard deviation for 3 separate measurements.

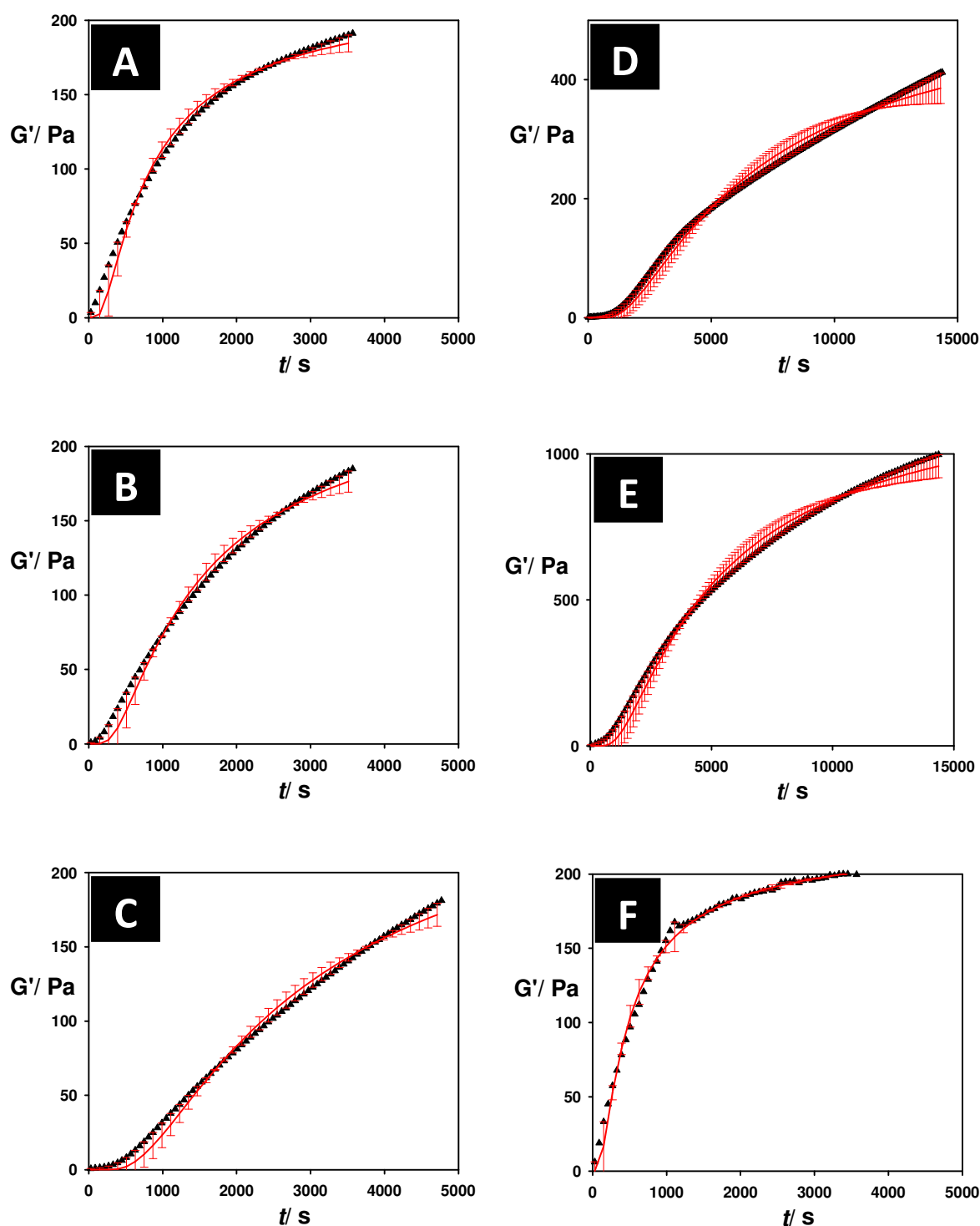


**Fig. S3.** Fits (red data points) of  $G' = G'_{inf} \exp(-B/t)$  to experimental data (black data points). The (red) error bars are the residuals. For clarity, only the fits to every 4th data point are shown. (A)  $C_{GEL} = 2.4$  wt.% plus  $C_E = 0.4$  mg ml<sup>-1</sup>; (B)  $C_{GEL} = 2.4$  wt.% plus  $C_E = 0.2$  mg ml<sup>-1</sup>; (C)  $C_{GEL} = 2.4$  wt.% plus  $C_E = 0.1$  mg ml<sup>-1</sup>; (D)  $C_{GEL} = 3.4$  wt.% plus  $C_E = 0.1$  mg ml<sup>-1</sup>; (E)  $C_{GEL} = 4$  wt.% plus  $C_E = 0.1$  mg ml<sup>-1</sup>. The SBP hydrogel in (F) was prepared from a different batch of SBP at  $C_{GEL} = 2$  wt.% and corresponds to SBP microgels imaged by CLSM and SEM in Figs. 5C and 5D, respectively.

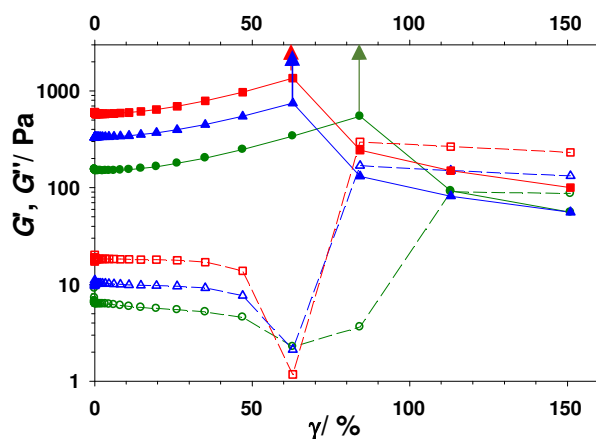


**Fig. S4.** Oscillatory shear amplitude sweeps performed on *quiescently* developed hydrogels at a frequency of 1 Hz:  $G'$  for  $C_{GEL} = 4\%$  (■),  $3.4\%$  (▲) and  $2.4\%$  SBP (●);  $G''$  open symbols of corresponding colour. SBP and laccase solutions were combined and added to the rheometer gap (1 mm), the sample trimmed and silicone oil (350 cSt) applied as a solvent trap. Hydrogels were allowed to develop for 2 (●) or 4 h (■ and ▲) prior to commencement of the measurements. The arrows indicate the arbitrary yield strain, taken as at the maximum in  $G'$ . These yield strain and corresponding yield stress values are: 84% and 460 Pa for  $C_{GEL} = 2.4$  wt.%, 63% and 747 Pa for  $C_{GEL} = 3.4$  wt.%; 63 % and 853 Pa for  $C_{GEL} = 4$  wt.%, also given in the text.

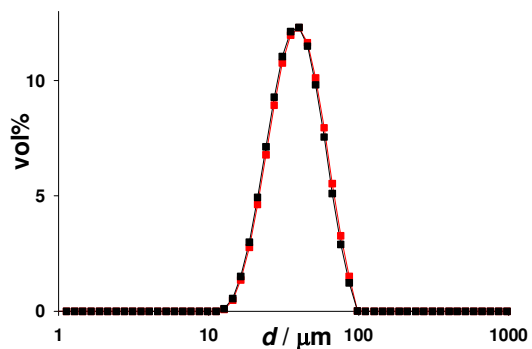


**Fig. S5.** PSD of non-heated (■) and heated (■) SBPM particles ( $C_{GEL} = 3.4$  wt.%). The latter sample was decanted into a plastic falcon tube and heated in a water bath at 85°C for 1 h then cooled to room temperature before re-sizing. The corresponding  $D_{32}$  values for the heated and unheated were 37.2 and 37.9 μm; the corresponding  $D_{43}$  values for the heated and unheated 43.0 and 43.8 μm, respectively.

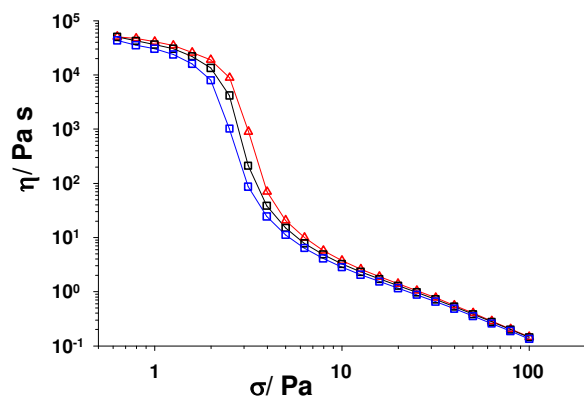


**Fig. S6.** Steady state viscosity curves for 3.4% SBPMG's ( $C_{PTOTAL} = 1.1$  wt.%) at three different gap heights; 1.1 mm ( $\blacktriangle$ ), 1 mm ( $\blacksquare$ ) and 0.9 mm ( $\bullet$ ). Each flow curve was performed using the same sample loading at progressively narrower gap heights.